Visual Evoked Potentials under High Rate Stimulation

Juan Manuel López

Thesis Advisor
Prof. Fredy Segura-Quijano

External Advisor
Prof. Jorge Bohórquez
University of Miami

Co-Advisor
Prof. Mario Valderrama
Universidad de los Andes

Co-Advisor
Prof. Juan Carlos Bohórquez
Universidad de los Andes

Thesis in partial fulfillment for the degree of
Philosophy Doctor in Engineering
Universidad de los Andes - Colombia
2017

Acknowledgments

The completion of this thesis could not have been possible without the assistance of my advisor committee. Thank you for all your support, timely advice, patience and guidance through all these years. Learning from you has been a privilege, which made me a better engineer and a better human being.

I am grateful to the Department of Electrical and Electronics Engineering of Universidad de los Andes and to the Administrative Department of Science, Technology and Innovation of Colombia (Colciencias) for their financial support.

I also want to thank to the Biomedical Engineering Department of the University of Miami for receiving me and for providing the main experimental tools for this work.

Finally, I want to thank my family for giving me their continued support and motivation during all my graduate school.

Contents

1 Introduction

Evoked Potentials (EPs) are the electrical responses of the nervous system after the presentation of an external sensory stimulus. Their amplitude tends to be small in comparison with other potentials like the spontaneous electroencephalogram (EEG) or the electrocardiogram (ECG), ranging from less than one microvolt to tens of microvolts. The clinical use of the evoked potentials is now common and serves in the identification of silent lesions, in monitoring changes and in the confirmation and localization of sensory abnormalities [1]. Three main types of EPs are widely used in clinical applications and research, these are: auditory evoked potentials (AEPs), visual evoked potentials (VEPs) and somatosensory evoked potentials (SEP). The main interest of this project is the study of VEPs, which are described below.

1.1 Visual Evoked Potentials

VEPs are the representation of the visual cortex response to a stimulation of the visual field. They allow the assessment of the optic nerves and the optic chiasm along with the areas of the brain in charge of receiving the visual information [2]. The International Society of Clinical Electrophysiology of Vision (ISCEV) provides a standard for clinical tests [3], indicating the experimental setup from the electrode montage to the nature of the stimulation.

VEPs are commonly recorded by placing EEG electrodes in the scalp, located in the occipital lobe (usually O_z, O_1 and O_2) referred to the frontopolar region (FP_z) or to the linked earlobes, as shown in Figure 1.1. For the signal acquisition, high amplification systems are used, along with filtering stages for noise reduction.

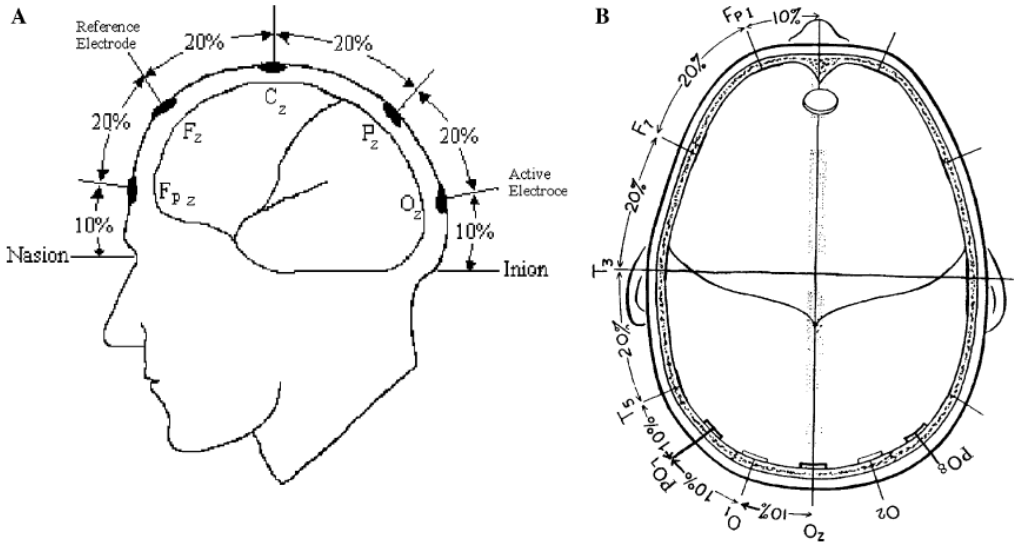

Figure 1.1. Electrode location for VEP recordings. Taken from [3]

Some remarks of the VEPs are [1], [3], [4]:

- They provide objective and reproducible observations
- Helps in the assessment of optic nerve in patients with subjective symptoms
- Cheaper technique in comparison with MRI
- They are not specific to a disease
- Are affected by age
- Requires cooperation from the patient to avoid noise

1.2 Types of Stimuli

Many types of stimulation exist, depending on the nature of the display (LED display, projectors, cathode ray tubes CRTs, handheld stroboscopic light, among others), the presentation (monocular or binocular) and the specific purpose of the test. Usually, the stimuli are delivered in a dimly illuminated room.

Types of stimulation are characterized by the following parameters [2]:

a) Stimulation field size: Specifies the size, in degrees, of the stimulation field. Usually, the field size must be bigger than 20°.
b) Pattern: Type of geometry of the elements of the stimulus. Squares, bars or gratings. For flash stimulation, no pattern is presented. Instead, the whole field size is illuminated for a given period.
c) Type of presentation: Indicates how the pattern is shown (does not apply to flash stimulation). There are two main cases, the pattern is changed or reversed, or the pattern appears.
d) Mean luminance: average of luminance computed as

$$L_{av} = (L_{max} + L_{min})/2 \qquad (1.1)$$

where $L_{\max}$ and $L_{\min}$ are the maximum and minimum luminance values of the field. Typical values of luminance, according to the standard, are 50 cd $^{m-2}$

e) Spatial frequency (f): is the number of variations (bars or gratings) in 1 degree. Is given in cycles per degree (cpd)
f) Constrast: Indicates the difference of luminance between black and white regions of the stimulation field size. Is computed according to

$$C = [(L_{max} - L_{min})/(L_{max} + L_{min})] \times 100\% \qquad (1.2)$$

The stimuli usually occupy a visual angle of 15° for the pattern–reversal and the pattern offset/onset, and about 20° or more for the flash stimuli.

There are three types of standard VEP stimulation: flash, pattern–reversal and pattern onset/offset. A brief explanation of the methods is given below.

1.2.1 Flash

Flash was the first type of stimulation used in the scientific and clinical context [1], [2]. It consists of a short flash with a duration of 5 ms or less. The flash stimulus must have a strength, which is the luminance integrated in time, ranging from 2.7 to 3.4 $\mathrm{cd} \cdot \mathrm{s} \cdot \mathrm{m}^{-2}$ [3]. The stimuli may be delivered by a handhelds stroboscopic light. Flash rate for clinical standard test is 1 Hz.

Although flash VEPs are more variable along subjects, they provide a tool to test visual pathways when there is no cooperation from the subject, since they do not depend on the attentional level [3].

Typical flash VEP is shown in Figure 1.2. Peaks are designated with "P" for positive and "N" for negative deflections, in ascending order in time, from the stimulus onset. The most prominent deflections are N2 and P2 occurring at approximately 90 ms and 120 ms respectively.

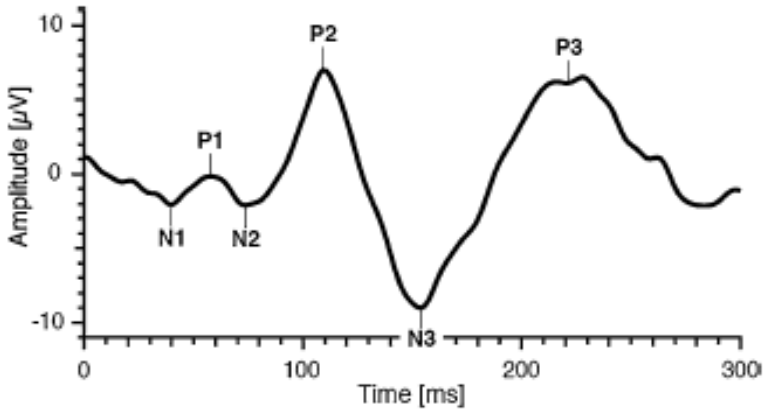

Figure 1.2. Typical VEP obtained with flash stimulation. Taken from [ISCEV]

The time of the deflections occurrence is called latency and is given in ms. Latency is one of the studied parameters in a clinical evaluation of the visual pathways, as will be discussed in section 1.4. Another important parameter is the amplitude of the main deflections. The amplitude of a wave is measured from the preceding deflection, for example, the amplitude of P2 is the height from N2 in microvolts.

1.2.2 Pattern-Reversal

Due to the preference of the visual system for edges and high-contrast geometries and movement, pattern-reversal stimulation is the preferred technique in the clinical field. The pattern-reversal stimuli consist of changing adjacent squares or bars from black to white at specific frequency in a display where the subject is asked to focus (see Figure 1.3). The total luminance of the stimuli must remain constant, implying that the same number of white and black squares or bars must be used. The contrast between black and white must be high, that is equal or greater than 80% [3]. The width of the lines or squares must be around 1°. The clinical most used stimulation rate is 2 reversal per second (rps), indicating two changes in the bars or squares. 1 rps is equivalent to 0.5 Hz, since Hz indicates a total cycle.

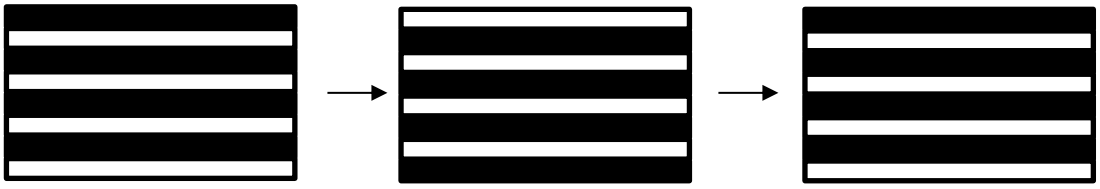

Figure 1.3. Example of a pattern reversal stimulus. One cycle is depicted

The pattern-reversal VEP is formed by three main waves: N75, P100 and N135. Figure 1.4 shows the shape of a typical pattern-reversal VEP.

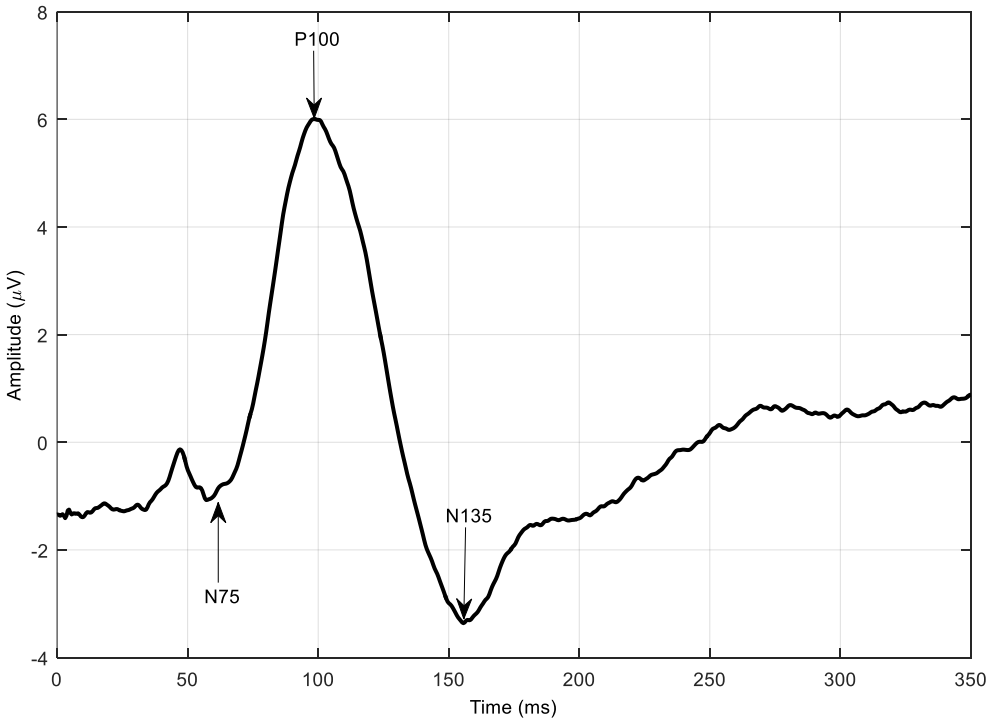

Figure 1.4. VEP generated after a pattern reversal stimulus. The stimulation frequency was 2 reversals per second (rps).

The characteristics of P100 (amplitude and latency) do not change significantly between healthy subjects and depend mainly on the stimuli features like luminance, pattern contrast, pattern size, among others. For this reason, laboratories must stablish their own standard values of amplitudes and latencies.

According to [2], [3], [5], [6], some subject variables, like age, sex and pupil size are also responsible for changes in the morphology of pattern-reversal VEPs. P100 latency increases with age while its amplitude is reduced. A possible explanation of this phenomenon is the reduction of the size of the pupil with the age [2], [5]. Additionally, females have a shorter P100 latency and lager amplitude

than males. In this sense, for clinical tests, each laboratory should have standard values of VEPs main features for each age group.

1.2.3 Pattern onset/offset

The pattern onset/offset stimulus consist of a brief exposure to a pattern (squares or bars), lasting 200 ms, called the "onset" followed by a longer period of a gray background, with a duration of 400 ms: the offset. The time distribution of these states assures, according to [3], that the response to the onset does not overlap with the response to the pattern offset.

The luminance in both cases, onset and offset, must remain the same to avoid a flash stimulus between the two states [5]. Pattern onset/offset VEPs exhibit more inter-subject variability than pattern-reversal VEPs, for this reason are only used in special cases like the diagnosis of albinism or patients with nystagmus [2], [3], [5].

Its form consists of three main deflections, as shown in Figure 1.5. Amplitude of each wave is measured with relation to its preceding deflection.

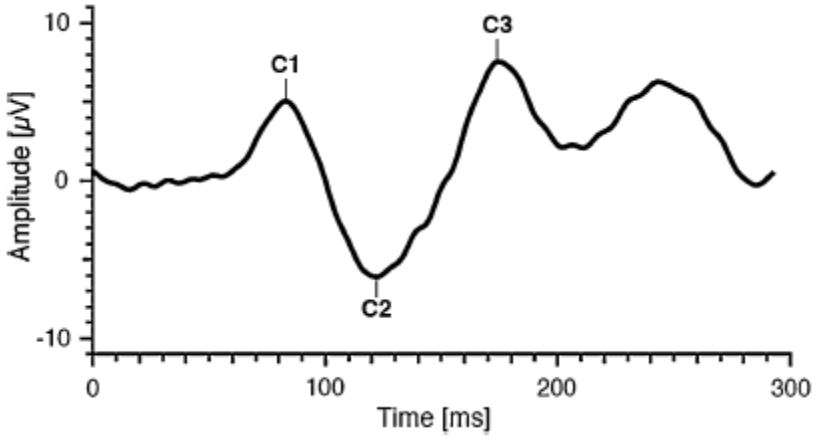

Figure 1.5. Pattern onset/offset VEP. Main deflections are denoted by C1, C2 and C3. Taken from [3]

1.3 Steady-State Evoked Potentials

When the stimulation rate is increased to more than 2 reversals per second (rps) for pattern-reversal visual stimulation, the response to one stimulus overlaps the response of the next stimulus, generating similar signals to those shown in Figure 1.6. These waves are called steady-state evoked potentials (SSEP) and were defined under the hypothesis that the brain follows the oscillation pattern of the stimuli, which is called brainwave entrainment. The mechanisms of the generation of these signals were thought to be different from those involved in the EPs since the brain possesses a high non-linearity.

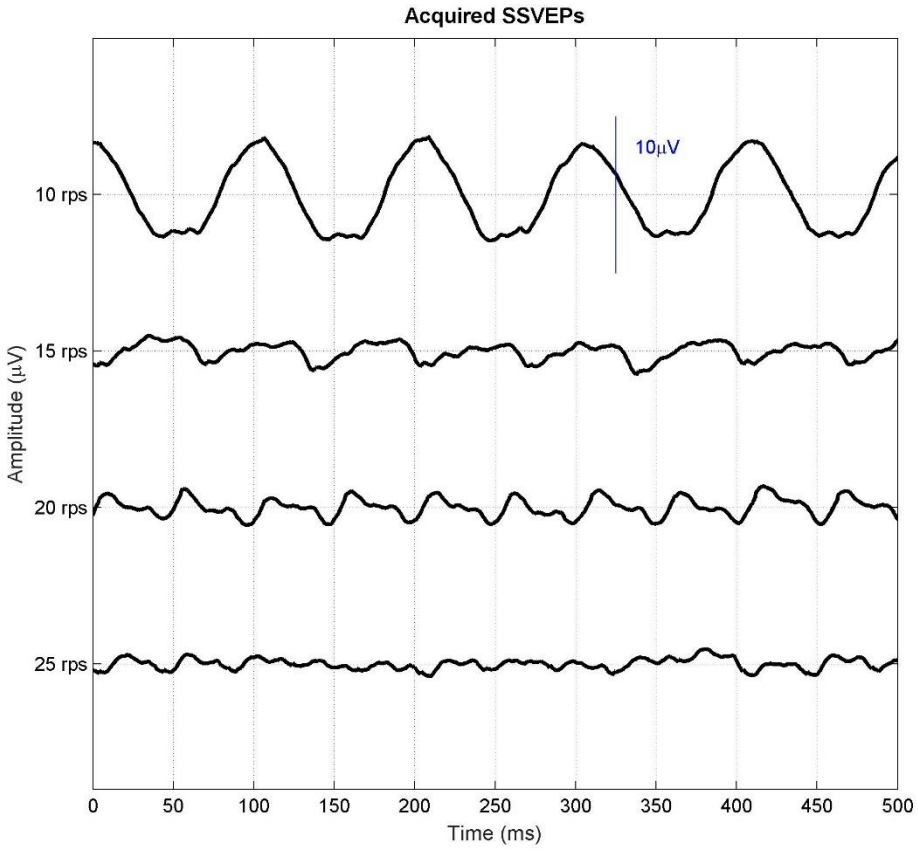

Figure 1.6. VEPs obtained for different stimulation rates. When the stimulation rate increases, individual responses overlap.

Recent works have shown, however, that the SSEPs can be explained as the linear superposition of individual EPs [7], [8]. A representation is shown in Figure 1.7, where final signal results from the summation of delayed individual responses.

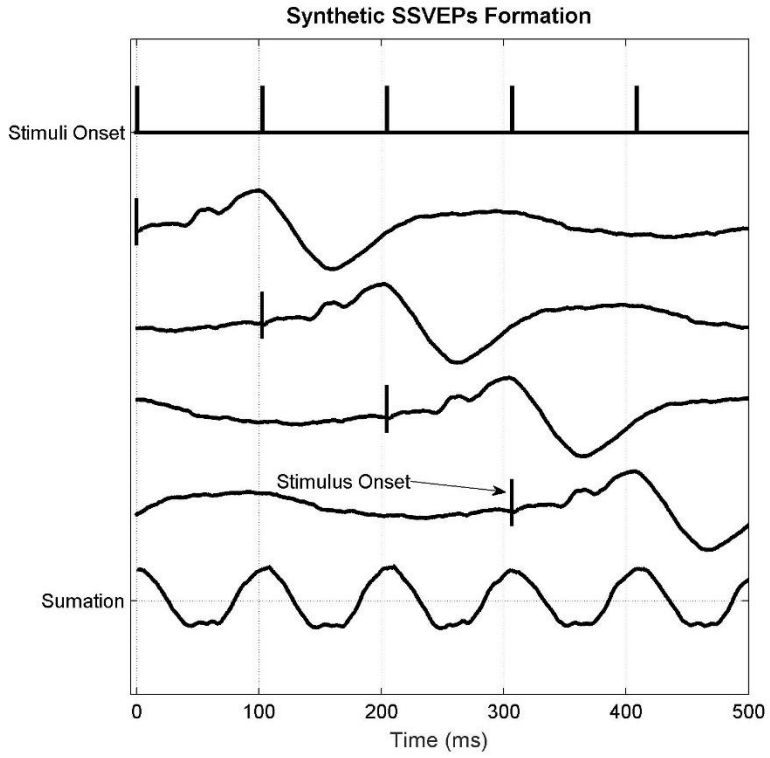

Figure 1.7. SSEP obtained from linear superposition of EP.

This new interpretation of SSEP broadens the exploration of the relationship of individual responses with high frequency stimulation and arise questions about time invariance of the brain responses and time resolution of the sensory mechanisms.

1.4 Some applications of VEPs

In the diagnostic of visual and neurodegenerative disorders, VEPs constitute a useful tool. Increment in latency and reduction in amplitude of P100 are the main clinical changes in the presence of disease. In addition, when using O_1 and O_2 channels, interhemispheric measurements can be done. Sometimes, these measurements are called "topographic analysis" [9]. Three main types of abnormalities can be distinguished: demyelinating, compressive and degenerative.

Demyelinating diseases (like Multiple Sclerosis MS) are characterized by asymmetric latency delays or severe latency delays. In the case of patients with MS, the VEPs are abnormal in 90% of them [1]. A compression of the optic nerve, glaucoma, amblyopia and ischemic optic neuropathy cause a diminishing in the amplitude of the VEPs, without a significant change in latency. According to [1], [9], abnormal VEPs can be observed even when vision is normal. For degenerative diseases, the VEPs change in symmetric manner, exhibiting latency delay without a significant decrement in amplitude [1].

Further investigations have looked for a relation between VEPs and particular neurological disorders like schizophrenia [10] and Alzheimer's disease (AD) [11]. Acceptable levels of specificity or significant differences in features of VEPs were found.

VEPs are also used for Brain-Computer Interfaces (BCI), where a human intention is translated into control signals for external devices, like wheelchairs, spellers, prosthesis, and orthoses, among others. Many investigations use SSVEPs, in this context, the main goal is the identification of stimulation frequency by the analysis of the EEG [12]–[16]. After identifying the frequency, a command is sent to the actuator to control the external device.

1.5 Scope of the Thesis

This project was oriented to the acquisition and analysis of brain activity, through EEG signals, and particularly, VEPs under high rate stimulation. To achieve this main aim, specific goals are described below

1.5.1 Design and implementation of human experiments for the study and characterization of VEPs at high rate stimulation

An experimental protocol was defined and implemented at the Neurosensory Laboratory of the University of Miami. Special montage and stimulation sequences were designed for the study of the VEPs, with stimulation frequencies ranging from 2 rps to 25 rps.

1.5.2 Study, analysis and characterization of VEPs generated under a high rate stimulation

With two novel techniques for VEP deconvolution called Continuous Loop Average Deconvolution (CLAD) and Least Square (LS), VEPs were analyzed for a healthy group of people, with ages ranging from 18 and 35 years old. Signals were examined in time, frequency and time-frequency domain.

1.5.3 Design and implementation of EEG acquisition systems

To provide Universidad de los Andes with tools to make further experimentation in VEPs, the creation of an EEG acquisition system was proposed. A total of three devices with a common hardware core were created for different experimental contexts. The family of devices is called "Brain Family" and consists of two wireless devices (Bluetooth and RF) and a third wired device, created for more demanding experiments, in sampling frequency, resolution and signal to noise ratio.

1.5.4 Design and implementation of a VDU for experimentation in humans

The VDU is responsible for the delivery of the stimuli to the subjects. As a part of this project, the development of such device was proposed. A two regions VDU was implemented to complete the toolbox for VEP studies at Universidad de los Andes.

1.6 Contributions

Three main findings are described in this document, regarding to the VEP analysis at high rate stimulation:

1.6.1 VEPs morphology changes, depending on the stimulus frequency.

Although some researchers have described the behavior of other evoked potential (see [7], [8], [17]–[19]), at the knowledge of the author, description of morphological changes related to frequency stimulation is scarce [20].

1.6.2 SSVEPs can be explained by linear superposition of individual responses.

The new techniques for VEP deconvolution allowed to test the hypothesis related to the linear superposition of individual responses to generate a SSVEP.

1.6.3 Brain elicited responses varies according to the nature of the stimulation sequence, for jittered sequences and isochronic sequences, mainly in the alpha band (8 – 12 Hz)

The time-frequency analysis shows that non-synchronic activity varies depending on the type of stimulation sequence, exhibiting mainly and increment in the alpha band for non-periodic, low-jittered sequences.

These contributions were detailed also in scientific paper called “Overlapped visual evoked potentials deconvolved at different stimulation rates”, summited on February 2 of 2017 to the Journal of Neural Engineering (IOP Publishing).

1.7 Organization of the document

This document is organized in chapters, as described below:

Chapter 2 is formed by a review of the state of the art, where an explanation of the main methods for EP extraction in the context of high stimulation rate is given. Three main techniques are detailed: Continuous Loop Deconvolution Average (CLAD), Burst Method, and Least-Squares Methods (LS). In addition, the importance of the new techniques in the clinical and non-clinical contexts are presented.

With these backgrounds, the reader will find in chapter 3, a description of the main experimentation performed during this project. VEPs were acquired from a group of healthy subjects, according to an experimental protocol including stimulation sequences at rates ranging from 2 rps to 25 rps. An analysis of the signals in time, frequency and time-frequency domain is presented. Principal features of the VEPs are described and compared for the explored techniques. Conclusions and future work for the project are presented.

In chapter 4, three designed systems for EEG acquisition are described. Details about hardware and software are provided. Specifications of the devices are compared with other commercial and research tools. Some performance tests and their results are shown.

At the end of the document, an annex explains the design and implementation of the VDU, which complements the EEG systems in the tasks of VEP acquisition.

1.8 References

[1] M. R. Nuwer, “Fundamentals of evoked potentials and common clinical applications today,” *Electroencephalogr. Clin. Neurophysiol.*, vol. 106, no. 2, pp. 142–148, Feb. 1998.

[2] G. E. Holder, G. G. Celesia, Y. Miyake, S. Tobimatsu, and R. G. Weleber, “International Federation of Clinical Neurophysiology: Recommendations for visual system testing,” *Clin. Neurophysiol.*, vol. 121, no. 9, pp. 1393–1409, Sep. 2010.

[3] International Society for Clinical Electrophysiology of Vision *et al.*, “ISCEV standard for clinical visual evoked potentials: (2016 update),” *Doc. Ophthalmol.*, Jul. 2016.

[4] P. Walsh, “The clinical role of evoked potentials,” *J. Neurol. Neurosurg. Psychiatry*, vol. 76, no. suppl_2, p. ii16-ii22, Jun. 2005.

[5] J. R. Heckenlively and G. B. Arden, *Principles and practice of clinical electrophysiology of vision*. Cambridge, Mass.: MIT Press, 2006.

[6] M. Kuba, J. Kremláček, J. Langrová, Z. Kubová, J. Szanyi, and F. Vít, “Aging effect in pattern, motion and cognitive visual evoked potentials,” *Vision Res.*, vol. 62, pp. 9–16, Jun. 2012.

[7] A. Capilla, P. Pazo-Alvarez, A. Darriba, P. Campo, and J. Gross, “Steady-State Visual Evoked Potentials Can Be Explained by Temporal Superposition of Transient Event-Related Responses,” *PLoS ONE*, vol. 6, no. 1, p. e14543, Jan. 2011.

[8] R. E. Delgado and O. Ozdamar, “Deconvolution of evoked responses obtained at high stimulus rates,” *J. Acoust. Soc. Am.*, vol. 115, no. 3, p. 1242, 2004.

[9] J. S. Ebersole, D. R. Nordli, and A. M. Husain, *Current practice of clinical electroencephalography*. 2014.

[10] M.-W. Huang, P.-Y. Lo, C.-H. Chen, C.-Y. Chen, and K.-S. Cheng, “The Application of Computerized WCST and Long-term Evoked Potentials for Schizophrenia Analysis,” 2006, pp. 5165–5168.

[11] Hsiao-Lung Chan, Wen-Chun Hsu, Ling-Fu Meng, and Mu-Hui Sun, “Event-related evoked potentials in Alzheimer’s disease by a tool-using gesture paradigm,” 2013, pp. 4299–4301.

[12] Yijun Wang, Xiaorong Gao, Bo Hong, Chuan Jia, and Shangkai Gao, “Brain-Computer Interfaces Based on Visual Evoked Potentials,” *IEEE Eng. Med. Biol. Mag.*, vol. 27, no. 5, pp. 64–71, Sep. 2008.

[13] Jinghai Yin, Derong Jiang, and Jianfeng Hu, “Design and application of brain-computer interface web browser based on VEP,” 2009, pp. 77–80.

[14] M. Spuler, “A Brain-Computer Interface (BCI) system to use arbitrary Windows applications by directly controlling mouse and keyboard,” 2015, pp. 1087–1090.

[15] L. Cao, Z. Ju, J. Li, R. Jian, and C. Jiang, “Sequence detection analysis based on canonical correlation for steady-state visual evoked potential brain computer interfaces,” *J. Neurosci. Methods*, vol. 253, pp. 10–17, Sep. 2015.

[16] U. Hoffmann, E. J. Fimbel, and T. Keller, “Brain-computer interface based on high frequency steady-state visual evoked potentials: A feasibility study,” 2009, pp. 466–469.

[17] F. Bardy, B. Van Dun, H. Dillon, and C. M. McMahon, “Deconvolution of overlapping cortical auditory evoked potentials recorded using short stimulus onset-asynchrony ranges,” *Clin. Neurophysiol.*, vol. 125, no. 4, pp. 814–826, Apr. 2014.

[18] J. Bohórquez and Ö. Özdamar, “Generation of the 40-Hz auditory steady-state response (ASSR) explained using convolution,” *Clin. Neurophysiol.*, vol. 119, no. 11, pp. 2598–2607, Nov. 2008.

[19] J. T. Valderrama, I. Alvarez, A. de la Torre, J. Carlos Segura, M. Sainz, and J. Luis Vargas, “Recording of auditory brainstem response at high stimulation rates using randomized stimulation and averaging,” *J. Acoust. Soc. Am.*, vol. 132, no. 6, p. 3856, 2012.

[20] J. Bohorquez, S. Lozano, A. Kao, J. Toft-Nielsen, and O. Ozdamar, “Deconvolution and Modeling of Overlapping Visual Evoked Potentials,” 2013, pp. 31–32.

2 Evoked Potential Estimation

Many methods have been proposed to retrieve the EPs from the signals containing the spontaneous EEG along with artefacts. Most recent works include the use of modern signal processing techniques (like wavelet analysis [1]–[5], support vector machines [6]–[8], artificial neural networks [9]–[11], among others). However, the goal of these new approaches has been to reduce the number of sweeps or single trials required for an acceptable signal-to-noise ratio (SNR) or new mechanisms for brain-computer interfaces.

A few approaches have explored the EPs under a high stimulation rate, by the creation of new stimulation protocols and mathematical techniques, allowing the extraction of individual responses from overlapped signals. In this chapter, three of these approaches are explained: Bursts method [12], Continuous Loop Averaging Deconvolution (CLAD) [13],and Least-Squares (LS) [14].

2.1 Linear Model

The signal of an electrode can be modeled as the weighted summation of different sources. Due to the volume conduction, the weights of the sources are smaller than one. A free of artifacts EEG data can be described by [15]

$$x_m(t,\ell) = \alpha_{m,1}(\ell)\cdot \mathcal{s}_1\ (t,\ell) + \alpha_{m,2}(\ell)\cdot \mathcal{s}_2\ (t,\ell) + \cdots + \alpha_{m,n}(\ell)\cdot \mathcal{s}_n\ (t,\ell) + \cdots$$

$$+\alpha_{m,N(\ell)}(\ell)\cdot \mathcal{s}_N\ (t,\ell) + \mathcal{v}_m\ (t,\ell) \qquad (2.1)$$

Where $m = 1,2,\dots,M$ is the number of the electrode; $t = 1,2,\dots,T$ is the number of the sample; $\ell = 1,2,\dots,L$ is the number of the single trial; $n = 1,2,\dots,N$ is the electrical source; $x_m(t,\ell)$ is the EEG data acquired at the electrode m; $\mathcal{s}_n\ (t,\ell)$ is the electrical source; $\alpha_{m,n}$ is the coefficient of the source n in the electrode m and $\mathcal{v}_m\ (t,\ell)$ represents the electrode noise.

It must be noted that sources $\mathcal{s}_n\ (t,\ell)$ may be stimulus-elicited or a spontaneous brain activity.

Under this model, the EP can be obtained by averaging the single trials data:

$$\hat{x}_m(t) = \frac{1}{L}\sum_{i=1}^{L} x_m(t,\ell)$$

$$= a_{m,1}\cdot s_1\ (t) + \cdots + a_{m,r}\cdot s_r\ (t) + \cdots + a_{m,R}\cdot s_R\ (t) + v_m(t) \qquad (2.2)$$

Where $\hat{x}_m(t)$ is the estimate of the EP at the location of electrode m; $r = 1,2,\dots,R$ is the number of the source; $s_r\ (t)$ is the enhanced phase-locked activity, spontaneous activity or a mixture of brain activities; $a_{m,r}$ is the coefficient between source r and electrode m and $v_m\ (t)$ is a mixture of electrode noise.

The complete procedure of extraction of the EP by averaging the acquired EEG signal is shown in Figure 2.1. An additional stage was added to reject those trials containing artifacts.

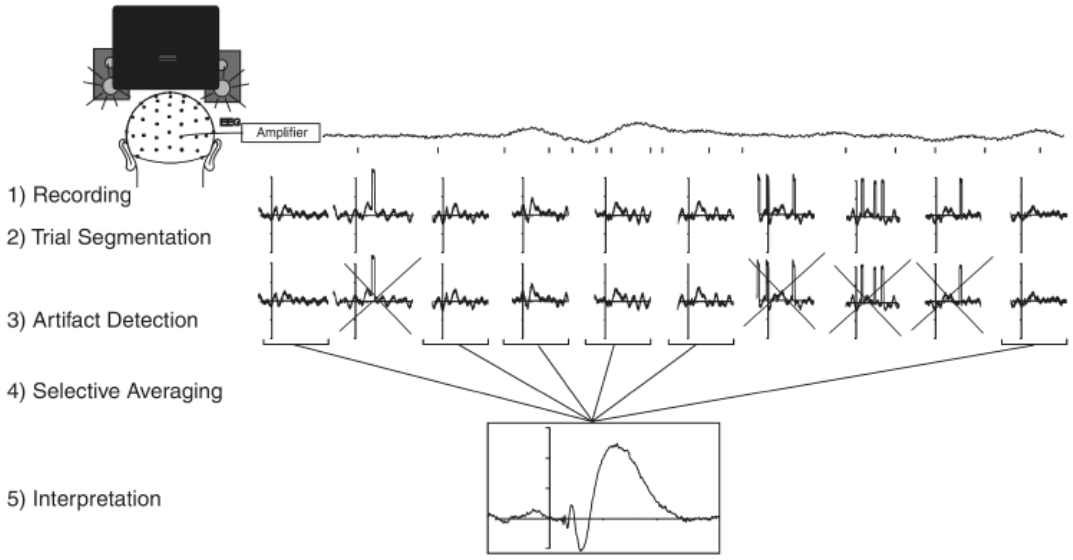

Figure 2.1 Method of Extraction of the EP by averaging. Taken from [15]

2.1.1 Assumptions of the linear model

According to [15], three main assumptions are made for the averaging:

a) EEG signal is artefact free.
b) The EEG data includes random spontaneous brain activity along with the constant elicited activity, which is synchronized with the stimuli.
c) The noise of the electrode is Gaussian.

In addition, EPs are assumed to remain stable during the experimentation, presenting no adaptation or other phenomena. This last assumption is also maintained for other EPs estimation techniques.

Under these assumptions, averaging will enhance the EP and decrease all other activities that are not phase-locked with the stimuli and the noise, providing enough single trials.

2.1.2 Problems of the linear model

The main flaws of the linear model rise from the following implications [15]:

- The number of sources must be equal though all trials, which is translated to $N(1) = N(2) = \cdots N(L) = R$
- The orders of electrical sources in any single trial are the same
- The sources of the EPs are estimated from $a_{m,n} \cdot s_n\ (t) = \frac{1}{L}\sum_{\ell}^{L} \alpha_{m,n}(\ell) \cdot s_n\ (t, \ell)$

The expression of equation (2.2) indicates then that the spontaneous brain activity is attenuated since it has different signs across the trials.

Some of the implementation problems, related to these assumptions, are described below:

- Adaptation may occur
- Is not possible to know if all electrical sources are involved in all single trials.
- EEG data will contain artifacts
- The EP from the averaging can have a significant part of brain activity not related with the stimulus, along with artefacts, and electrode noise
- Is not possible to analyze overlapping signals (when the stimulation frequency is high and individual responses overlap)

To overcome these issues, other approaches have been proposed. The first explored technique, burst method, may provide information about adaptation for VEPs, the second technique, CLAD, deals with the deconvolution problem when an overlapped response is obtained, and the third technique, LS, have the non-periodic property, avoiding effects of periodicity of the sequence.

2.2 Burst Method

This approach was designed by Özdamar et al. [12] to measure adaptational effects in EPs, particularly in pattern electroretinograms (PERG) and VEPs under high rate stimulation (9.8 rps). It consists on deliver "bursts" to the subject. The bursts are formed by a sequence of stimuli, ranging from one to eight stimuli

Bursts are arranged randomly in a sequence, lasting 118 s. The sequence is presented 12 times (12 trials) to the subjects for a total acquisition time of 24 minutes. After the acquisition, bursts with the same number of stimuli are averaged to enhance the synchronized response and weak the spontaneous activity along with the noise, as explained in section 2.1. To obtain individual responses, waveforms are subtracted and shifted, as illustrated in Figure 2.2.

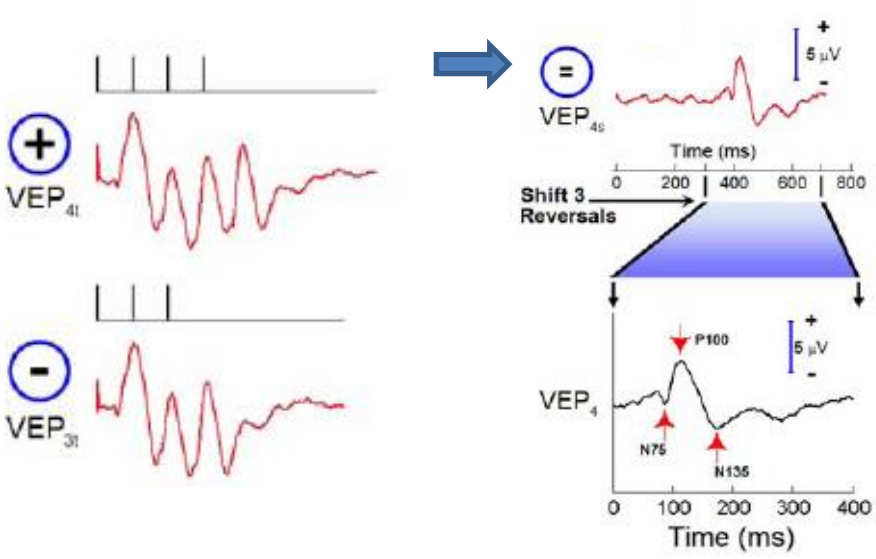

Figure 2.2 Unit responses (EPs) from the subtraction of consecutive responses. The signal shown in the second row is subtracted from the signal of the first row, resulting in the unit response shown in the third row. Figure adapted from [12]

For the experimentation, Özdamar et al. used a population of 10 subjects, with normal vision. Results of this experiment show a rapid adaptation for PERG and variations in the VEPs, however, the work lacks a statistical analysis validating these differences. Figure 2.3 shows the results.

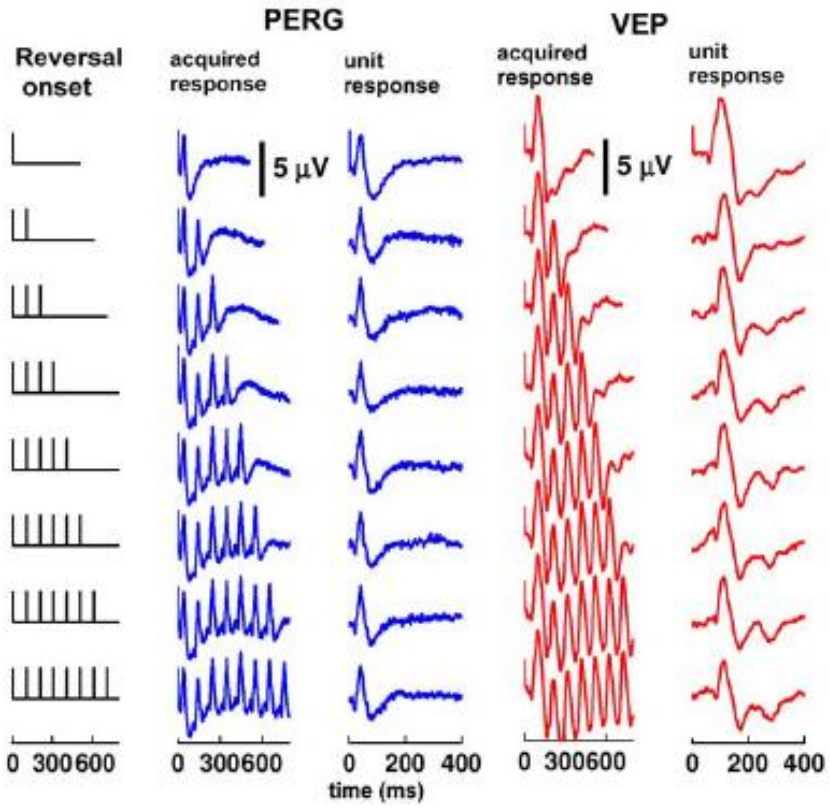

Figure 2.3. Population averages of PERG and VEPs. Individual responses are shown in column 3 and column 5. Taken from [12].

Amplitude and latency differences can be noticed in both signals, PERG and VEP. The authors attributed the observed differences to the vasculature in charge of the neural visual structures. To formulate a better hypothesis, more experimentation is required, for example, with different stimulation rates, or different stimulation sequences. Although this simple method is promising, no further related investigations has been formulated, to the best knowledge of the author.

2.3 Continuous Loop Averaging Deconvolution (CLAD)

Motivated by the work of Eysholdt and Schreiner [16], the Continuous Loop Averaging Deconvolution (CLAD) proposed by Delgado and Özdamar [13] provides a mechanism to obtain deconvolved responses from the analysis of a signal composed by overlapping EPs.

The key feature of this method is the presentation of a non-isochronic sequence of stimuli at high rates, causing overlapping in the responses and a signal like the SSEP, which is called “the convoluted response” (see Figure 2.4 C).

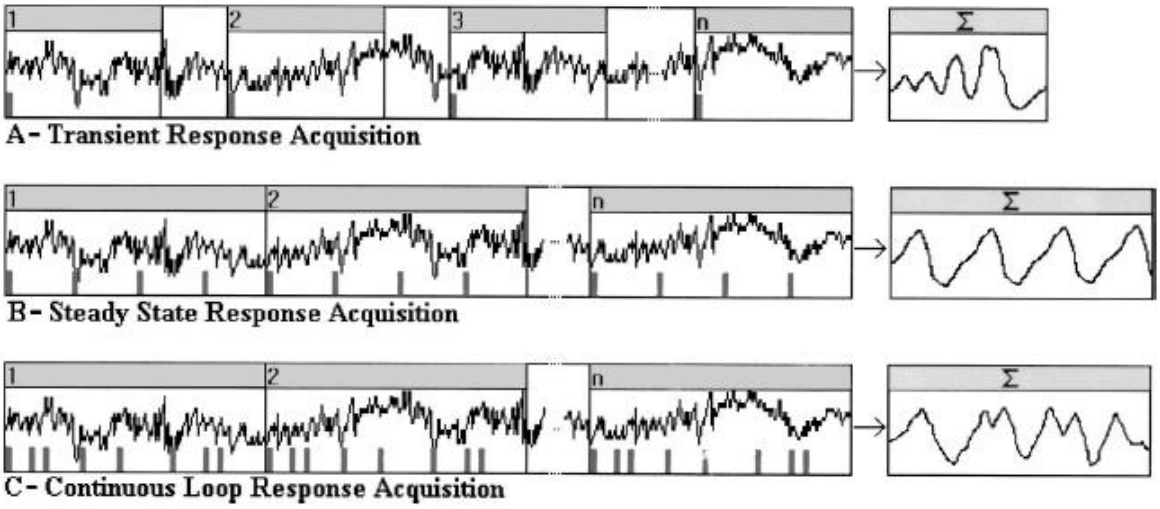

Figure 2.4. Comparison of different types of responses. A. Transient response, caused by low stimulation rates. B. Steady-State response (SSEP), elicited by high stimulation rates and C. CLAD response which reassembles the SSEP, but with some differences due to the nonisochronic nature of the sequence. Figure taken from [13].

2.3.1 Assumptions

In the same fashion than for the linear model, for this method two main assumptions are made [13]:

a) Individual responses are independent to each other.
b) The convoluted response is the sum of the overlapped individual responses

In the development of this method, an averaging stage is also required to improve the SNR and weak the spontaneous brain activity. Along with the previously described assumptions, some of the items shown in section 2.1.1 are also valid here. The difference with the conventional averaging is that in this case, the whole response of one sequence is averaged, instead of only one response to an individual stimulus.

2.3.2 Deconvolution

CLAD deconvolution can be explained in time domain [13] or in frequency domain [17]. Here, the frequency domain approach will be detailed, since it is more compact and provides an efficient implementation by means of the fast Fourier transform.

Under a high stimulation rate, since the individual responses are overlapped, the signal acquired (after averaging) will be

$$x(t) = \sum_{i=1}^{L} a(t - t_i\ ) + n(t) \qquad (2.3)$$

Where $a(t)$ is the individual response to one stimulus, $n(t)$ is the residual noise and L is the number of individual trials or sweeps for a given sequence. From equation 2.3, one may think of $x(t)$ as a circular signal composed by a summation of shifted versions of the same wave $a(t)$.

$x(t)$ can be interpreted as the convolution of $a(t)$ with the stimulus sequence function $s(t)$.

$$v(t) = a(t) * s(t) + n(t) \qquad (2.4)$$

Applying Fourier transform, the equation 2.4 can be expressed as

$$V(f) = A(f)S(f) + N(f) \qquad (2.5)$$

The computation of $A(f)$ can be done using arithmetic methods. Therefore, the response in time can be obtained with

$$\hat{a}(t) = \mathcal{F}^{-1}\left(\frac{V(f)}{S(f)} - \frac{N(f)}{S(f)}\right) \text{ if } [S(f) \neq 0] \forall f \qquad (2.6)$$

From equation 2.6 is deduced that the selection of the stimulus sequence is crucial to obtain good quality estimations of the EP. The Fourier transform of $s(t)$ cannot be zero for any frequency, implying that isochronic stimulation cannot be used with the CLAD method. The inverse of $H(f) = 1/S(f)$ is called "deconvolution filter" and provides information about noise characteristics in the deconvolution process. Figure 2.5 explains graphically convolution and deconvolution processes.

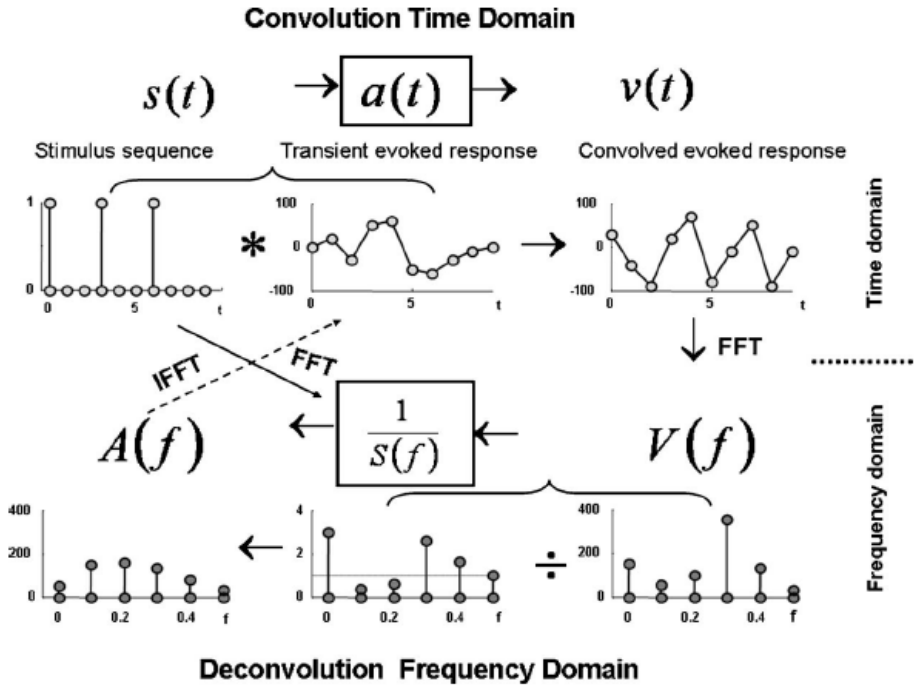

Figure 2.5. Convolution and deconvolution of signals in time and in frequency domains. Figure taken from [13]

A block diagram shows the deconvolution mechanism in Figure 2.6. Both, the sequence and the acquired signal, are processed by the Fourier transform. An estimation of the EP in frequency is obtained and the last stage consists on using the inverse Fourier transform.

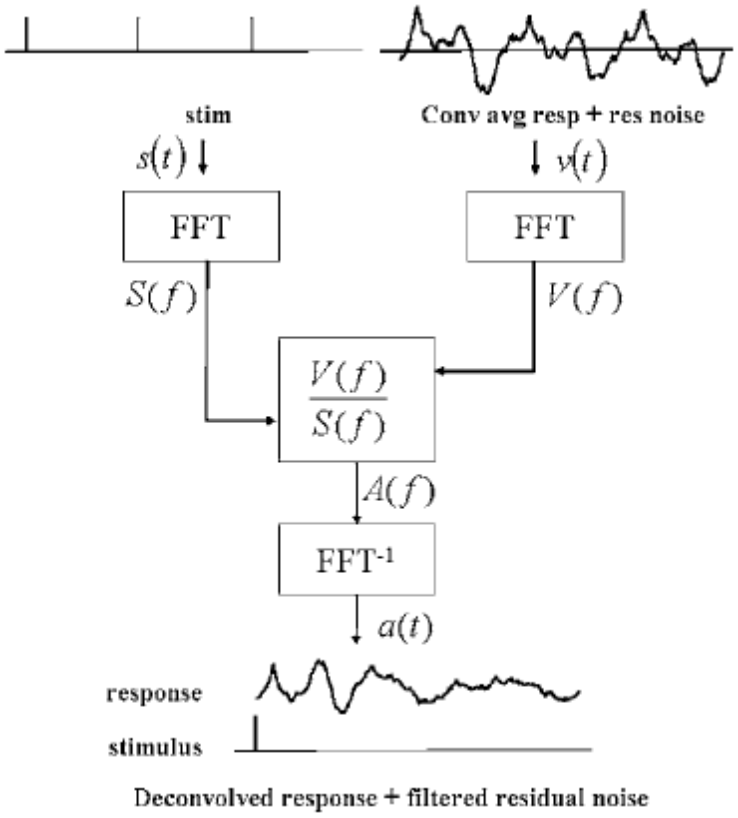

Figure 2.6. Deconvolution process. Sequence and signal are converted to the frequency domain by the Fourier transform. An estimation of the frequency response of the EP is obtained and the response in time is computed with an inverse Fourier transform. Taken from [13].

2.3.3 Signal-to-Noise Ratio for CLAD

The deconvolution process does not alter the EP, but may cause noise attenuation or amplification, depending on the form of $H(f)$. Following this consideration, the SNR may be defined by the ratio of the signal amplitude and the noise amplitude[13]:

$$SNR_{amp} = \frac{\sigma_s}{c_g\ \sigma_n} \qquad (2.7)$$

Where c_g is the gain due to any noise reduction process.

From averaging, the noise is reduced by a factor of $1/\sqrt{K}$, but in addition, effects of the deconvolution must be accounted:

$$c_g = c_{dec}c_{avg} = c_{dec}\left(\frac{1}{\sqrt{K}}\right) \qquad (2.8)$$

Assuming constant frequency components for noise, and using Parseval's theorem [13]:

$$c_{dec} = \sqrt{\frac{1}{F}\sum_{i=1}^{F} H(f)H^*(f)} \qquad (2.9)$$

Where F is the Nyquist frequency. The magnitude of $H(f)$ is analyzed to obtain the noise gain factor. $H(f)$ must be less than one for noise attenuation. SNR for the deconvolution is:

$$SNR_{tot} = \frac{1}{\sqrt{K}} \frac{\sigma_s}{c_{dec}\sigma_n} \qquad (2.10)$$

2.3.4 CLAD Method Studies

First works with this technique aimed the validation of the method and its capability of retrieve EPs in real time. Examples of these early investigations are [13], [17], [18], and the studied EPs were auditory EPs (AEPs), although Delgado and Özdamar [13] remarked the fact that CLAD can be used in a variety of applications beyond EP estimation.

An interesting contribution using CLAD was provided by Bohórquez and Özdamar [18], where a 40 Hz Auditory Steady-State response (ASSR) was explained by the superposition of auditory brainstem responses (ABRs) and middle latency responses (MLRs) providing evidence of the superposition hypothesis (see section 1.3) for the human auditory system.

Presacco et al. [19] studied the relationship between ASSR and ABR, MLR, gamma band responses (GBR) and beta band responses (BBR). They used two methods to assess this relationship: a modified CLAD and a last click response method (LCR). CLAD showed good results at predicting ASSR except for the onset part of the signals, while LCR failed in both portions of (onset and steady-state) of the signals.

Özdamar et al. [20] studied the morphology of MLRs under high stimulation rates, and observed a significant change of the Pb deflection, showing a “resonance” at approximately 40 Hz, consistently with the high amplitude of ASSR at the same stimulation frequency.

For the human visual system, Capilla et al. [21] studied the CLAD technique with VEPs, finding a strong resemblance between the SSVEPs and the synthetic SSVEPs generated from the deconvolved responses. However, the deconvolution technique is not clearly explained. This job constitutes the first one, as the best knowledge of the author, in applying CLAD method (or a similar method) to the visual system. Shows the obtained SSVEPs from [21].

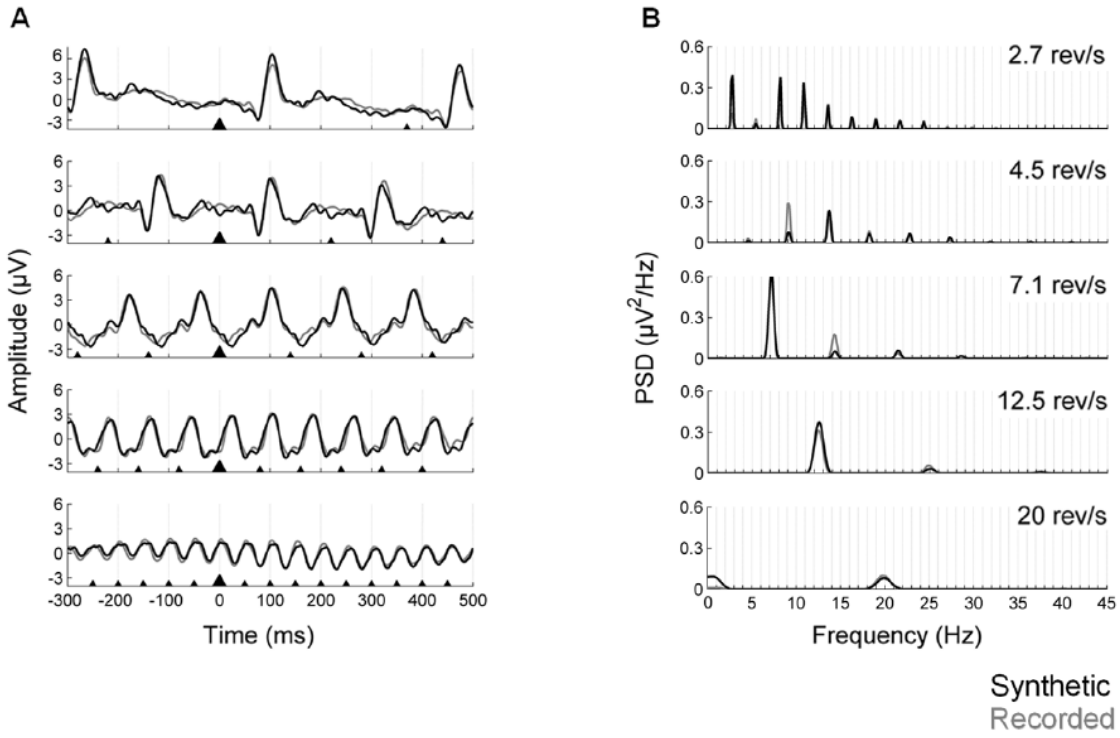

Figure 2.7. Synthetic waveforms from superposition of individual responses. Black lines correspond to synthetic signals and gray lines correspond to recorded signals. A) signals in time, B) Power Spectrum Density of the waveforms. Taken from [21]

Bohórquez et al. [22] investigated the VEPs deconvolution using two different stimulation rates: 8.2 rps and 13 rps. The results show a consistency between synthetic SSVEP and recorded SSVEP. Figure 2.8. Population averages for five conditions: Isochronic slow stimulation rate at 1.6 Hz, two jittered conditions at 13.0 Hz and 8.2 Hz and two isochronic high rate stimulation at 8.2 Hz and 13 Hz. A shows population averages. B exhibits the deconvolved responses. C Shows the synthetic waveforms created by superposition of the deconvolved responses. shows the waveforms obtained from six young adults. There is no statistical analysis to conclude that synthetic SSVEPs and recorded SSVEPs are not different from each other.

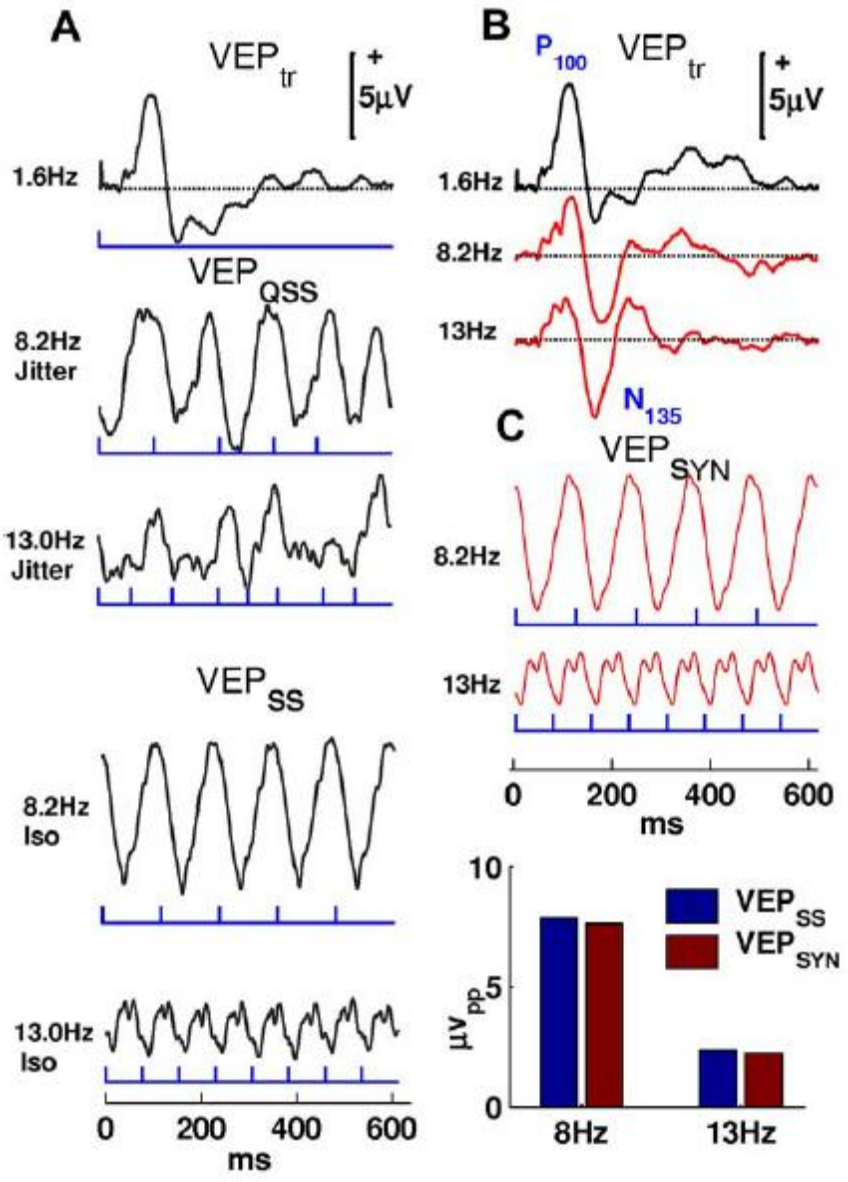

Figure 2.8. Population averages for five conditions: Isochronic slow stimulation rate at 1.6 Hz, two jittered conditions at 13.0 Hz and 8.2 Hz and two isochronic high rate stimulation at 8.2 Hz and 13 Hz. A shows population averages. B exhibits the deconvolved responses. C Shows the synthetic waveforms created by superposition of the deconvolved responses. Taken from [22]

Finally, a few explorations of related techniques were presented by Wang et al. [23], [24], where stimulation sequences are generated independently from the sampling frequency of the EEG acquisition system.

From this short review, it is noticeable that the focus of EPs and CLAD related investigations were aimed to analyze the auditory system. A deeper exploration with the human visual system must be done, varying, for example, the stimulation rate, analyzing not only the phase-locked responses but also the induced responses that may be caused by different process from the visual pathways and

providing more evidence related to the superposition hypothesis. This thesis aims to answer at some extent this necessity.

2.4 Least-Squares (LS) Deconvolution Method

Through the CLAD method, the deconvolution of evoked responses comes from periodic stimulation sequences, which are averaged before the individual VEP extraction. This requirement comes from the necessity of reduce noise. CLAD analysis in frequency domain is simple and allows the design of stimulation sequences with an adequate noise reduction [17]. However, the periodicity of these sequences may affect the acquired response, especially the one related to cognitive processes.

To assess this hypothesis, a new kind of non-periodic sequences is required, with a similar stimulation histogram than CLAD. Least-Squares (LS) method emerged from this rationale [25].

2.4.1 Assumptions and Computation

The assumptions are the same as with CLAD: the evoked response is identical for each stimulus (time-invariant) and the spontaneous EEG is not correlated with such response. In this context, $s(k)$ is a non-periodic sequence (long enough), and $y(k)$ is the acquired signal. The evoked response is a_j and has a finite length L.

The evoked potential for the kth sample will be the superposition of the previous stimulus response including in a window with L samples. In this way, the convoluted signal can be written as:

$$\hat{y}(k) = \sum_{j=0}^{L-1} a_j \;\; s(k-j) \qquad k = L, L+1, \dots, N \qquad (2.11)$$

Hence, deconvolution goal is to find a set of a_j , $j = 0,1, \dots, L-1$ minimizing the mean square error:

$$E = \sum_{k=L}^{N-1} \big(\hat{y}(k) - y(k)\big)^2 \qquad (2.12)$$

N is the total number of acquired samples. Equation 2.12 may be written as:

$$E = \sum_{k=L}^{N-1} \Big(\sum_{j=0}^{L-1} a_j \;\; s(k-j) - y(k)\Big)^2 \qquad (2.13)$$

To minimize the error, a set of coupled equations is posed, having the form

$$\frac{\partial E}{\partial a_i} = 0,\ i = 0, 1, \dots L-1 \qquad (2.14)$$

Applying 2.14 in 2.13, the equation set becomes:

$$\sum_{j=0}^{L-1} a_j \;\; \sum_{k=L}^{N-1} s(k-i)s(k-j) = \sum_{k=L}^{N-1} s(k-i)\, y(k) i = 0, 1, \dots, L-1 \qquad (2.15)$$

Matrix notation allows that equation 2.15 can be expressed as:

$$\begin{bmatrix} \sum_k s(k)s(k) & \sum_k s(k)s(k-1) & \dots & \sum_k s(k)s(k-(L-1)) \\ \sum_k s(k-1)s(k) & \sum_k s(k-1)s(k-1) & \dots & \sum_k s(k-1)s(k-(L-1)) \\ \dots & \dots & \dots & \dots \\ \sum_k s\big(k-(L-1)\big)s(k) & \sum_k s\big(k-(L-1)\big)s(k-1) & \dots & \sum_k s\big(k-(L-1)\big)s(k-(L-1)) \end{bmatrix} \begin{bmatrix} a_0 \\ a_1 \\ \dots \\ a_{L-1} \end{bmatrix} = \begin{bmatrix} \sum_k s(k)y(k) \\ \sum_k s(k-1)y(k) \\ \dots \\ \sum_k s\big(k-(L-1)\big)y(k) \end{bmatrix} \quad (2.16)$$

EP can be obtained from equation 2.16. Given that the involved matrix, in the linear equations, depends only on the sequence, it can be computed only once and the result can be used to further make a deconvolution process in a more efficient way.

When the sequence is long enough, the following approximations can be made:

$\sum_{k=L}^{N-1} s(k-i)s(k-i) \approx \sum_{k=L}^{N-1} s(k)s(k)$ and

$$\sum_{k=L}^{N-1} s(k-i)s(k-i-j) \approx \sum_{k=L}^{N-1} s(k)s(k-j)\; i,j = 0,1,\dots,L-1 \quad (2.17)$$

Hence, equation 2.16 becomes:

$$\begin{bmatrix} r_{ss}(0) & r_{ss}(1) & \dots & r_{ss}(L-1) \\ r_{ss}(1) & r_{ss}(0) & \dots & r_{ss}(L-2) \\ \dots & \dots & \dots & \dots \\ r_{ss}(L-1) & r_{ss}(L-2) & \dots & r_{ss}(0) \end{bmatrix} \begin{bmatrix} a_0 \\ a_1 \\ \dots \\ a_{L-1} \end{bmatrix} = \begin{bmatrix} r_{sy}(0) \\ r_{sy}(1) \\ \dots \\ r_{sy}(L-1) \end{bmatrix} \quad (2.18)$$

Where:

$$r_{ss}(i) = \sum_{k=L}^{N-1} s(k)s(k-i),\; i = 0,1,\dots,L-1 \quad (2.19)$$

Y

$$r_{sy}(i) = \sum_{k=L}^{N-1} y(k)s(k-i),\; i = 0,1,\dots,L-1 \quad (2.20)$$

EPs can be estimated through the matrix invers or solving directly the linear system using equations 2.16 or 2.18.

2.4.2 LS studies

Bardy et al. [14] tested this method on auditory evoked potentials in a population formed by eleven adults with a broad age range (from 19 to 55 years old), using tone-burst stimuli of 500 and 2000 Hz. The stimulus onset-asynchronies (OSA) jittered around 150, 250, 450, and 850 ms.

They found important differences depending on the jitter used in the sequences: amplitudes reduced near to the 450 ms jitter. In addition, the alternation of stimulus frequency increased the amplitude of the AEPs. The differences are explained by a model of latent inhibition.

As the best knowledge of the author, there is no other related work with LS and particularly VEPs. In this thesis, LS method is compared with CLAD.

2.5 References

[1] Y. Erkan and N. Acir, “Wavelet denoising of middle latency response in auditory evoked potentials,” 2011, pp. 631–634.

[2] H. Drissi, F. Regragui, J. . Antoine, and M. Bennouna, “Wavelet transform analysis of visual evoked potentials: some preliminary results,” *ITBM-RBM*, vol. 21, no. 2, pp. 84–91, Apr. 2000.

[3] I. Rejer, “Wavelet Transform in Detection of the Subject Specific Frequencies for SSVEP-Based BCI,” in *Hard and Soft Computing for Artificial Intelligence, Multimedia and Security*, vol. 534, S. Kobayashi, A. Piegat, J. Pejaś, I. El Fray, and J. Kacprzyk, Eds. Cham: Springer International Publishing, 2017, pp. 146–155.

[4] R. H. J. van der Lubbe, I. Szumska, and M. Fajkowska, “Two Sides of the Same Coin: ERP and Wavelet Analyses of Visual Potentials Evoked and Induced by Task-Relevant Faces,” *Adv. Cogn. Psychol.*, vol. 12, no. 4, pp. 153–167, Dec. 2016.

[5] M. R. Mowla, S.-C. Ng, M. S. A. Zilany, and R. Paramesran, “Single-Trial Evoked Potential Estimation Using Iterative Principal Component Analysis,” *IEEE Sens. J.*, vol. 16, no. 18, pp. 6955–6960, Sep. 2016.

[6] D. Aminaka, S. Makino, and T. M. Rutkowski, “SVM classification study of code-modulated visual evoked potentials,” 2015, pp. 1065–1070.

[7] S. Tayeb, A. Mahmoudi, F. Regragui, and M. M. Himmi, “Efficient detection of P300 using Kernel PCA and support vector machine,” 2014, pp. 17–22.

[8] Y. Wang and Y. Hu, “Identifying the location of spinal cord injury by support vector machines using time-frequency features of somatosensory evoked potentials,” 2016, pp. 1–5.

[9] M. Alfaro-Ponce, A. Argüelles, and I. Chairez, “Pattern recognition for electroencephalographic signals based on continuous neural networks,” *Neural Netw.*, vol. 79, pp. 88–96, Jul. 2016.

[10] J. Sato and Y. Washizawa, “Neural decoding of code modulated visual evoked potentials by spatio-temporal inverse filtering for brain computer interfaces,” 2016, pp. 1484–1487.

[11] Xu-Sheng Zhang, R. J. Roy, D. Schwender, and M. Daunderer, “Discrimination of anesthetic states using midlatency auditory evoked potentials and artificial neural networks,” 2000, vol. 2, pp. 1383–1386.

[12] O. Ozdamar, B. D. Yilmaz, O. Villalon, and J. Bohorquez, “Adaptation Dynamics Measures in Simultaneously Recorded Pattern Electroretinograms and Visual Evoked Responses,” 2013, pp. 11–12.

[13] R. E. Delgado and O. Ozdamar, “Deconvolution of evoked responses obtained at high stimulus rates,” *J. Acoust. Soc. Am.*, vol. 115, no. 3, p. 1242, 2004.

[14] F. Bardy, B. Van Dun, H. Dillon, and C. M. McMahon, “Deconvolution of overlapping cortical auditory evoked potentials recorded using short stimulus onset-asynchrony ranges,” *Clin. Neurophysiol.*, vol. 125, no. 4, pp. 814–826, Apr. 2014.

[15] F. Cong, T. Ristaniemi, and H. Lyytinen, *Advanced signal processing on brain event-related potentials: filtering ERPs in time, frequency and space domains sequentially and simultaneously*. Hackensack, NJ: World Scientific, 2015.

[16] Eysholdt, U. and S. Schreiner, C. C., “Maximum length sequences—A fast method for measuring brainstem evoked responses,” *Audiology*, vol. 21, no. 3, 1982.

[17] Ö. Özdamar and J. Bohórquez, “Signal-to-noise ratio and frequency analysis of continuous loop averaging deconvolution (CLAD) of overlapping evoked potentials,” *J. Acoust. Soc. Am.*, vol. 119, no. 1, p. 429, 2006.

[18] J. Bohórquez and Ö. Özdamar, “Generation of the 40-Hz auditory steady-state response (ASSR) explained using convolution,” *Clin. Neurophysiol.*, vol. 119, no. 11, pp. 2598–2607, Nov. 2008.

[19] A. Presacco, J. Bohórquez, E. Yavuz, and Ö. Özdamar, “Auditory steady-state responses to 40-Hz click trains: Relationship to middle latency, gamma band and beta band responses studied with deconvolution,” *Clin. Neurophysiol.*, vol. 121, no. 9, pp. 1540–1550, Sep. 2010.
[20] Ö. Özdamar, J. Bohórquez, and S. S. Ray, “Pb(P1) resonance at 40Hz: Effects of high stimulus rate on auditory middle latency responses (MLRs) explored using deconvolution,” *Clin. Neurophysiol.*, vol. 118, no. 6, pp. 1261–1273, Jun. 2007.
[21] A. Capilla, P. Pazo-Alvarez, A. Darriba, P. Campo, and J. Gross, “Steady-State Visual Evoked Potentials Can Be Explained by Temporal Superposition of Transient Event-Related Responses,” *PLoS ONE*, vol. 6, no. 1, p. e14543, Jan. 2011.
[22] J. Bohorquez, S. Lozano, A. Kao, J. Toft-Nielsen, and O. Ozdamar, “Deconvolution and Modeling of Overlapping Visual Evoked Potentials,” 2013, pp. 31–32.
[23] T. Wang, C. Zhan, G. Yan, J. Bohórquez, and Ö. Özdamar, “A preliminary investigation of the deconvolution of auditory evoked potentials using a session jittering paradigm,” *J. Neural Eng.*, vol. 10, no. 2, p. 026023, Apr. 2013.
[24] T. Wang, J. Huang, L. Lin, and C. A. Zhan, “Continuous- and Discrete-Time Stimulus Sequences for High Stimulus Rate Paradigm in Evoked Potential Studies,” *Comput. Math. Methods Med.*, vol. 2013, pp. 1–10, 2013.
[25] F. Bardy, H. Dillon, and B. Van Dun, “Least-squares deconvolution of evoked potentials and sequence optimization for multiple stimuli under low-jitter conditions,” *Clin. Neurophysiol.*, vol. 125, no. 4, pp. 727–737, Apr. 2014.

3 Visual Evoked Potentials Under High Stimulation Rates

In this chapter, the application of the "continuous loop averaging deconvolution" (CLAD) and "least-squares" (LS) methods is extended to the visual evoked potentials (VEPs). The elicited, non-synchronic, brain responses caused by the stimulus sequences is investigated.

Four periodic and four non-periodic jittered pattern-reversal sequences at different main rates (9.80, 14.92, 19.60 and 25.00 reversals per second) were presented to seven healthy subjects (males, 20 to 30 years old). Overlapping VEPs were deconvolved using the CLAD and the LS methods. VEPs at 2.00 rps and SSVEPs at the same stimulus rates used for the jittered sequences were additionally acquired. Signals were examined in the time, frequency and time-frequency domains.

Deconvolved VEPs exhibited variations, consistent across all subjects, in their morphology, depending on the stimulus frequency. SSVEPs could be reconstructed using the individual deconvolved responses, from the two methods used, with no statistical differences when compared with the acquired SSVEPs. Time-frequency domain and phase synchronization analysis of the acquired signals revealed differences in the brain responses between isochronic and jittered sequences for all subjects, particularly at the gamma band (30 to 55 Hz).

Deconvolved VEPs showed strong coherence across all the studied subjects, validating the CLAD and the LS methods for the visual system. SSVEPs at the studied stimulus frequencies are formed by the linear superposition of individual responses. The elicited responses in the primary visual cortex depend not only on the stimulus rate but also on the nature of stimulation sequence (jittered or isochronic). Visual responses to high stimulus rate may provide objective and new information about the function of the visual pathway and the processing carried out by the visual cortex. Time-frequency and phase synchronization results may be correlated to high-level processes, such as perception.

3.1 Introduction

VEPs are used in the diagnosis of neuro-ophthalmic diseases such as optic neuritis, optic neuropathy, ocular hypertension, glaucoma, multiple sclerosis (MS), among others. Regarding the steady-state VEPs (SSVEPs), they are often used in brain-computer interfaces (BCI) applications, since they exhibit a better classification accuracy than other methods such as P300 and event-related desynchronization/synchronization [1], [2]. Given the current importance of VEPs in the clinical and in the research fields, a study of the VEPs at high stimulus rate may not only broaden the knowledge of the mechanisms behind the visual cortex processes, but also may lead to new valuable methods to gather information regarding integrity of visual pathways.

The study presented in this chapter aimed the characterization of high stimulus rate VEPs of healthy subjects, by using the methods of deconvolution of evoked responses "continuous loop averaging deconvolution" (CLAD) and "least-squares" (LS), explained in chapter 2.

3.2 Explanation of the Experiment

For a set of stimulus rates, overlapped VEPs were extracted using the frequency domain CLAD method described [3], and the LS method described by [4]. In addition, SSVEPs were obtained to analyze and compare the signals in the three cases.

3.2.1 Subjects

For this study, 7 male adults (ages ranging from 21 to 30 years) with normal or corrected to normal vision and no history of photosensitive epilepsy or other neurological disorder, participated in the study. According to the Code of Ethics of the World Medical Association, a written informed consent was obtained from the participants with the approval of the Institutional Review Board of the University of Miami.

3.2.2 Stimuli

Pattern-reversal stimuli were delivered to the subjects in a dimmed room, using a specially designed LED VDU with ten horizontal bars with a total field size of 33° x 38°, a bar size of 3°, mean luminance of 150 cd m-2 and a contrast ratio greater than 98% [5].

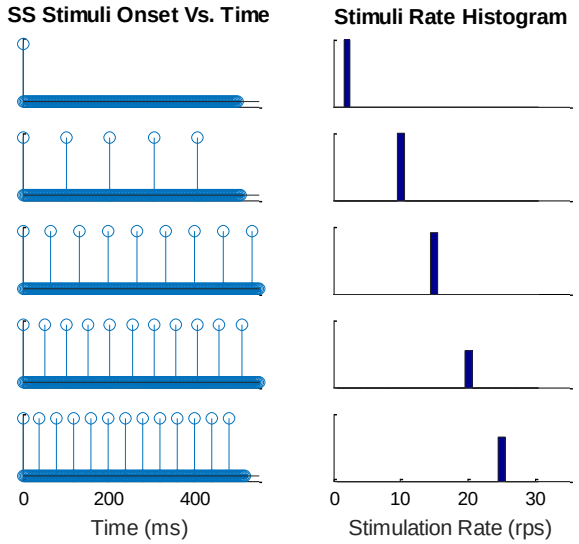

Figure 3.1. Sequences used in the experiment. A. SS sequences. The histogram shows the isochronic nature of these sequences

Four periodic, low-jitter sequences were designed at main stimulus rates of 10, 15, 20 and 25 rps. These sequences exhibit a good frequency response to avoid noise amplification as stated by Özdamar and Bohórquez [3]. Four non-periodic, low-jitter sequences were additionally designed at the same main stimulus rates, according to the LS technique from Bardy et al., [4]. In order to acquire SSVEPs, isochronic sequences were designed at 2.00 rps and at 9.80, 14.92, 19.60 and 25.00 rps. In Figure 3.1, the sequences are depicted along with their inter stimuli intervals (ISI) histograms. LS stimuli onset versus time was cropped at 450 ms due to the length of the sequence.

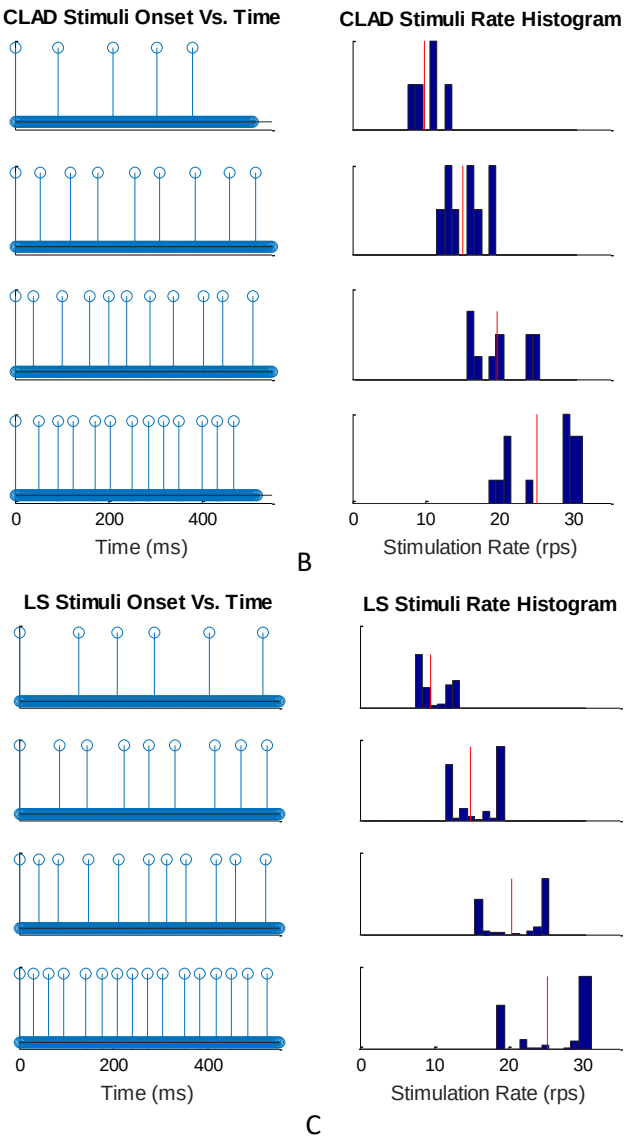

Figure 3.1. (Continued) Sequences used in the experiment. B. CLAD sequences. The histogram shows more than one rate; the red line marks the average stimulation rate. C. LS sequences. For these sequences, the time axes was cropped at 450 ms, since the total length was more than 1 minute. The red line in the histograms is the mean stimulation rate of the sequence.

For the periodic and the isochronic sequences, each sequence was repeated 128 times to form a stimulation train. For the non-periodic sequences, each train was formed by one presentation of the sequence. Trains were presented to the subjects in an organized manner, first the trains of the isochronic sequences and then the trains of the jittered sequences.

None of the stimulation trains exceeded a time duration of 1.5 minutes. A complete presentation of all possible sequences and rates constitutes a trial. Three trials were acquired per subject. Before the stimulation, a gray pattern was shown at the display for at least 30 seconds to ensure a non-adaptational state. After each stimulation train, subjects could rest from viewing at the VDU for as

long as they want, and during these pauses, the gray pattern was shown again in the VDU. Figure 3.**¡Error! No se encuentra el origen de la referencia.** describes the composition of the trials.

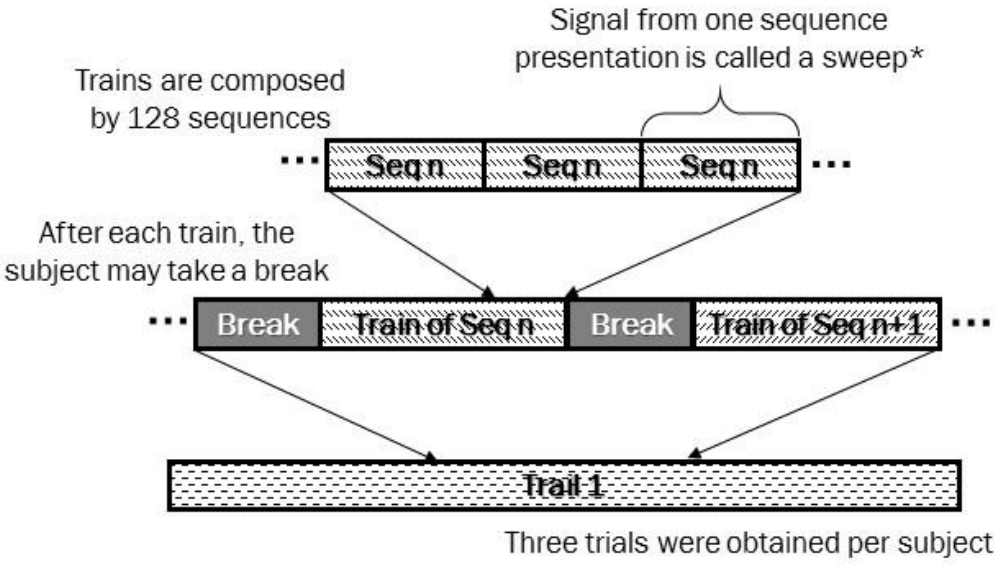

Figure 3.2 Composition of the trials. Each trial was composed by trains. The trains were packages of sequences for the SS and CLAD sequences, and for just one sequence in the LS case.

3.2.3 Experimental setup

Electrophysiological signals were acquired with a Smart-EP acquisition system (Intelligent Hearing Systems, Miami, FL). One channel was used, locating the electrodes at Oz (+) and Fz (-) with the ground located on the forehead (Fpz) according to the International 10-20 system [6]–[8]. The sampling frequency was set to 2000 samples per second (SPS), the analog gain was 100 k and the filter bandwidth was set to 1 Hz to 300 Hz (-3dB).

EEG conductive paste was used to assure low impedance (less than 5 kΩ) across the electrodes. During the experiment, the non-dominant eye of the subjects was occluded with an eyepatch to take into account only one visual pathway per subject. Subjects were sitting comfortably in a dimmed booth, with their chins over a chinrest at 25 cm from the VDU. The subjects were instructed to fix their view at the center of the display, where a small mark was located.

3.3 Analysis

Acquired signals were imported to MATLAB (Mathworks) for further analysis. VEPs from the periodic and the non-periodic low-jitter sequences were deconvolved for each subject, and their latencies and amplitudes were analyzed. For artifact rejection, any signal sweep with a peak-to-peak amplitude greater than 30 μV was removed. Population averages are shown in Figure 3.2 (left), where the main VEP peaks (N75, P100 and N135 according to [7]–[9]) can be clearly distinguished. SSVEPs were extracted through the classical approach of averaging the sweeps, applying the same artifact rejection threshold of 30 μV; these signals can be seen in Figure 3.2 (right).

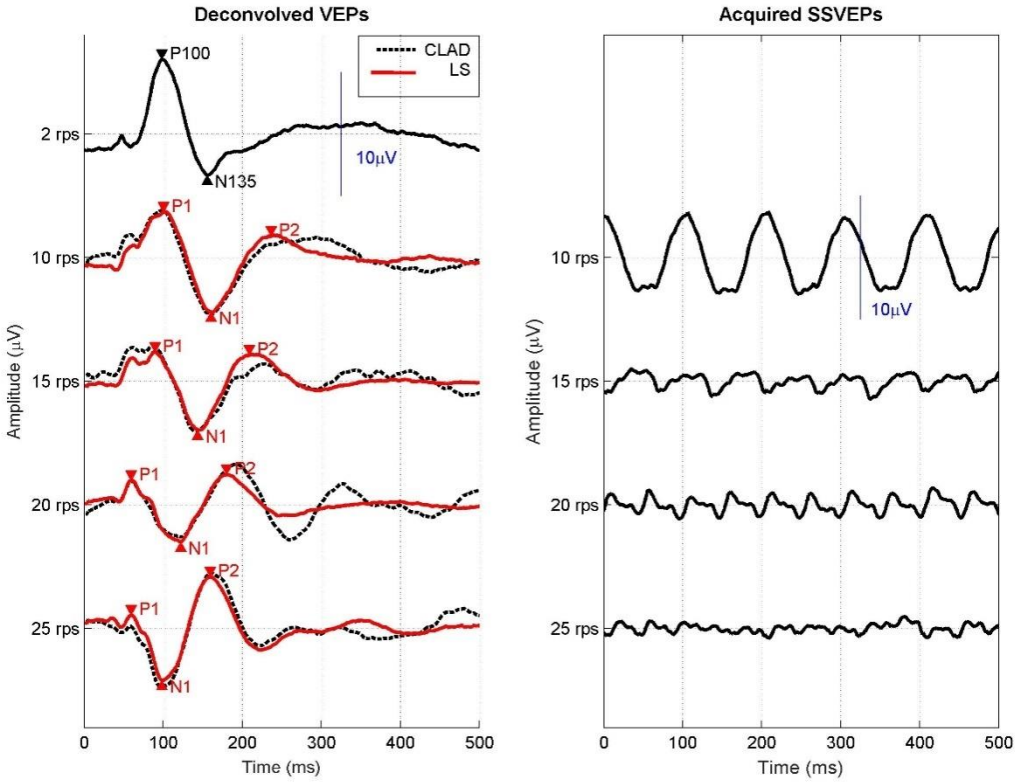

Figure 3.2 Deconvolved VEPs using CLAD and LS methods. At the lefts, results for the deconvolution process can be observed, while in the right, the SSVEP are shown

Synthetic SSVEPs were created from the extracted VEPs, according to each stimulus frequency. Resulting signal is formed by the linear superposition of the individual responses, organized per the stimulus sequence, as illustrated in Figure 1.7 in chapter 1. This procedure allowed a comparison between the synthetic and the acquired SSVEPs.

A time-frequency domain analysis was performed using a Gabor wavelet [10] for 500 scales, representing a pseudo-frequency range from 1 to 100 Hz. For this case, the wavelet transform was computed first for each sweep of data, and then averaged for each condition. By doing this, activities not synchronized with the stimuli (induced activities) could be observed in the resulting mean scalogram. Due to the non-periodic nature of the LS sequence, the length of the sweep used for averaging was chosen to be similar to those on the periodic sequences. Additionally, a phase synchrony index was computed using the method described in [11]. In this method, the wavelet transform is computed, and the phase information is extracted. The aim of the processes mentioned above was to stablish a difference between the activities elicited by the jittered sequences and the isochronic sequences.

3.4 Statistical analysis

Permutation tests were performed, according to [12], [13], allowing an objective comparison between inter-individual signals and between the nature of the sequences (jittered vs. isochronic). Briefly, the permutation method consists on the following steps:

1. Formation of a single set of data with the two experimental conditions.

2. Selection of two subsets. The first subset must contain the same number of samples for the first condition, selected in a random fashion. The second subset must contain the remaining samples. Use these subsets to obtain the test statistic.

3. Repeat step two a large number of times to obtain a histogram of the test statistic.

4. Make a comparison of the test statistic from the original sets with the obtained histogram from step three. The p-value is obtained by computing the number of partitions with a larger test statistic larger than the original.

5. If the p-value is smaller than the alpha-level (chosen to be 0.05 for this research), the data in the two conditions are significantly different.

Monte Carlo approximation for the tests presented in this document, was done with 3000 iterations (repetition of step 2).

3.5 Results

3.5.1 Deconvolved VEPs

Deconvolved VEPs for each subject are shown in Figure 3.3. Inter-individual differences in amplitude and latency of the deflections were observed, but the morphology (number of deflections and approximated latency) of the signals was consistent across subjects. The main deflections of the VEPs change, depending on the stimulation frequency, in the same fashion for all the subjects. Table 1 summaries the average peak-to-peak amplitudes of the most prominent deflection and peak latencies.

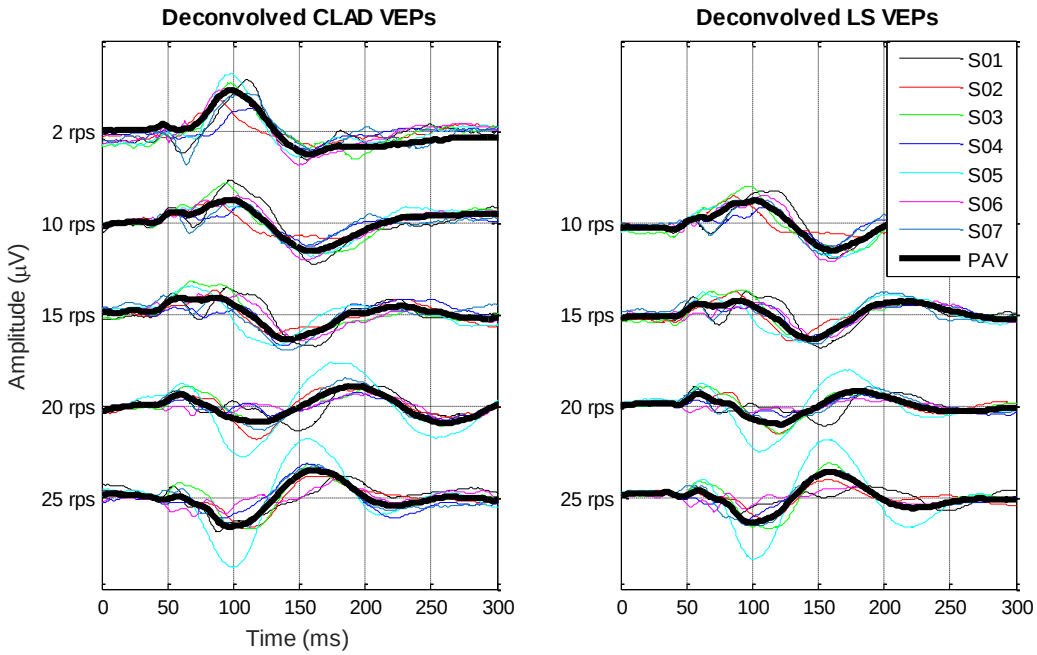

Figure 3.3 Deconvolved VEPs. The right figure shows the deconvolved signals obtained with the CLAD method. The dark line indicates the average signal over all the subjects. In the left, LS method was applied.

Amplitudes and latencies showed no statistical difference across the two deconvolution methods ($p > 0.05$, permutation tests; Table 3.1) In Figure 3.2 the main deflections were identified as P1, N1 and P2, avoiding the use of their latencies due to their change with the stimulation rate. The main positive deflection reduced its amplitude and latency when the stimulation frequency increased. For 20 rps and 25 rps, a second positive deflection was more prominent between the 150 ms and the 200 ms; and the negative deflection, usually located at 135 ms, occurs between 90 ms and 120 ms.

Table 3.1 Peak-to-peak amplitudes and latencies, depending on the stimulation frequency

Stim. Rate (rps)	Type	P1-N1		P2-N1		P1		N1		P2	
		Amplitude (μV)	p-value	Amplitude (μV)	p-value	Latency (ms)	p-value	Latency (ms)	p-value	Latency (ms)	p-value
10	CLAD	8.39	0.68	6.98	0.99	100.1	0.23	158.6	0.23	249.6	0.4
	LS	8.12		6.99		102		161.5		238.5	
15	CLAD	6.89	0.67	7.18	0.9	86.1	0.62	142.6	0.98	227.6	0.3
	LS	6.32		6.99		88.5		143.5		221.5	
20	CLAD	4.47	0.93	7.48	0.64	59.6	0.25	123.6	0.35	194.6	0.1
	LS	4.99		6.57		59.5		122		181	
25	CLAD	4.96	0.99	10.62	0.51	57.6	0.87	97.1	0.49	159.6	0.95
	LS	5.27		8.94		59.5		98.5		159.5	

3.5.2 Synthetic SSVEPs and acquired SSVEPs

Figure 3.6 shows the population averages and their power spectral densities (PSD) of the synthetic SSVEPs and the acquired SSVEPs. No major differences can be observed in time or frequency domain, especially at stimulus rates below 20 rps. A linear correlation analysis showed significant correlation between the synthetic SSVEPs and the acquired SSVEPs for a significance level of 0.05. These results indicate that SSVEPs may be formed by the superposition of individual VEPs, as discussed in other works for VEPs and for auditory evoked potential (AEPs) [14]–[16]

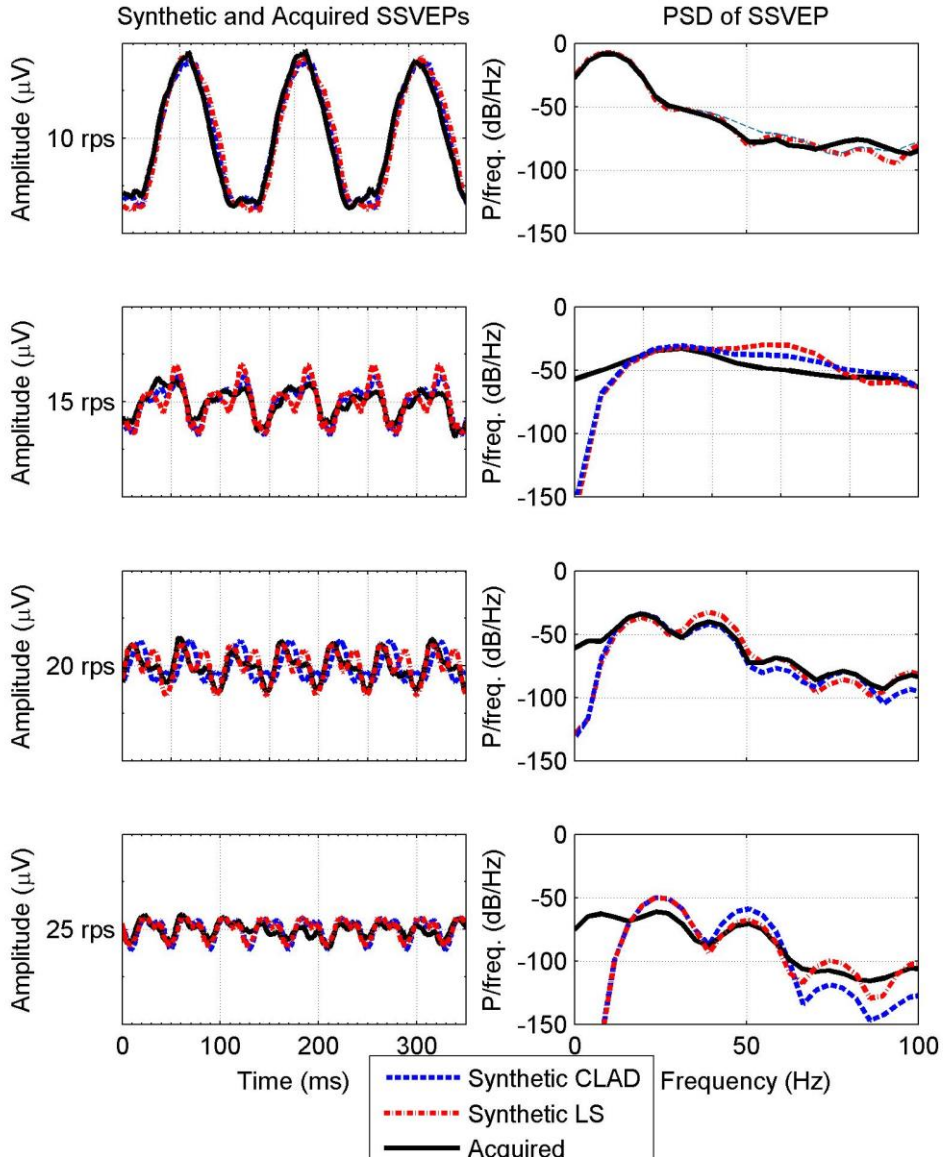

Figure 3.6 Population average of synthetic SSVEPs. Comparison in time and in frequency domain are shown.

3.5.3 Time-frequency domain

Brain activity was analyzed by frequency bands and for each subject. Figure 3.7 shows the average scalogram for the alpha band where differences in the power of the signal can be observed. The

analysis in the time-frequency domain showed a marked difference in the brain activity between low-jittered and isochronic sequences. A greater activity could be observed in the alpha band (8-12 Hz) for the non-periodic, low-jittered sequences, except for the case of the sequences at 10 rps, where isochronic sequences exhibited more power that the CLAD and LS sequences.

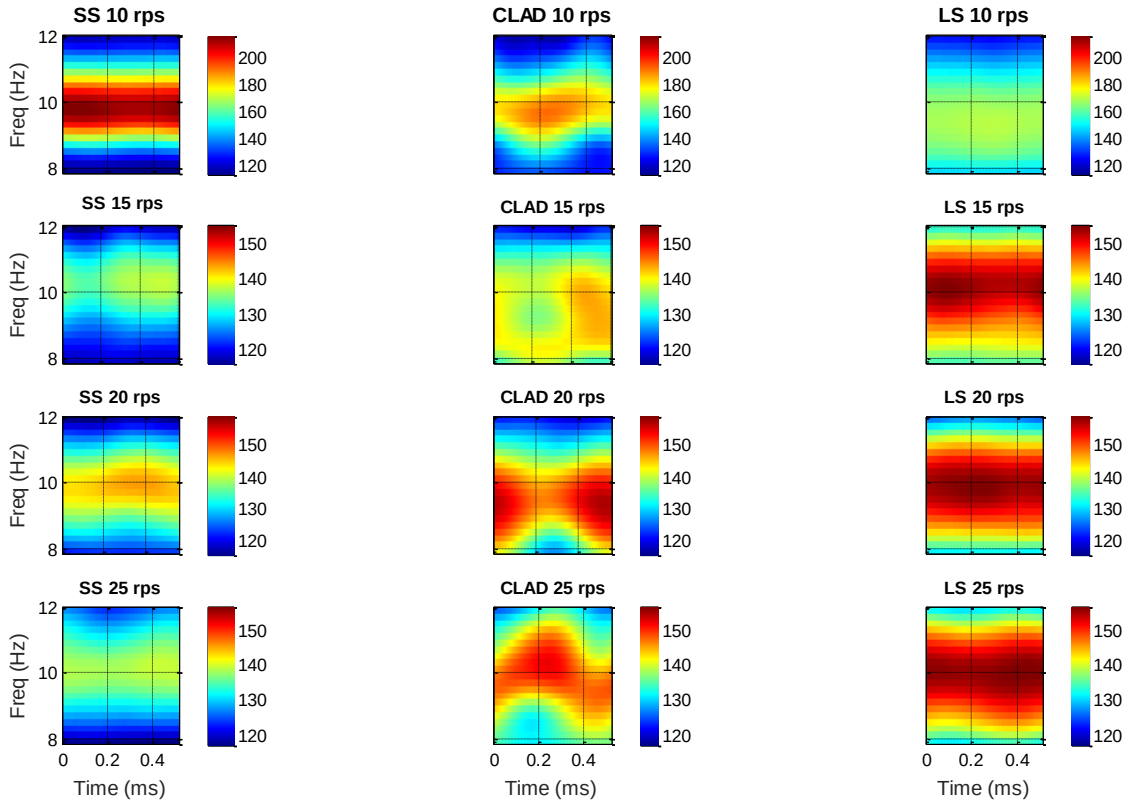

Figure 3.7 Population average scalogram for alpha band. Color limits are the same for each stimulation frequency, allowing a visual comparison

Another difference was observed in the theta band (4-8 Hz) for all stimulation rates, where more power was observed for LS and CLAD than for the SS sequences. All differences described were statistically significant ($p < 0.05$, permutation test). Figure 3.8 shows a bar plot of the average power for theta and alpha bands. Symbols above the bars indicate if the values were statistically different.

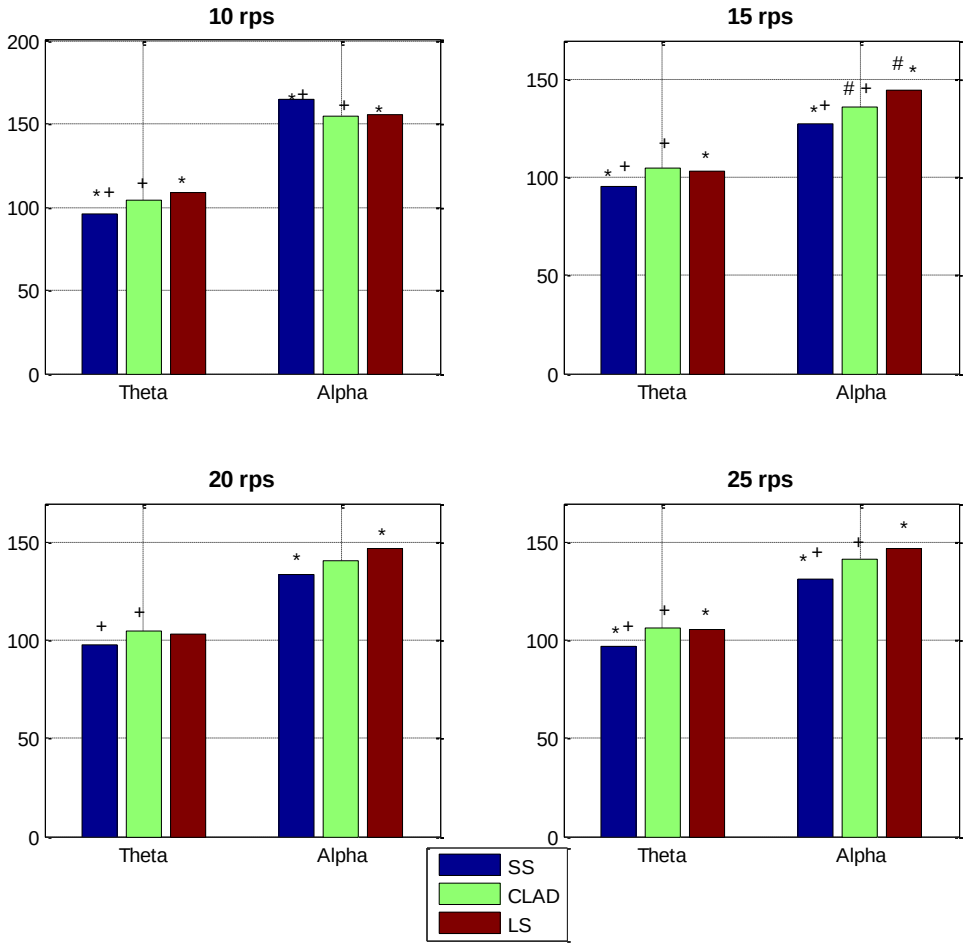

*Figure 3.8 Bar plot for Theta and Alpha bands. * mark means a statistical difference between SS and LS, + mark indicates a statistical difference between SS and CLAD and # indicates a difference between CLAD and LS*

3.6 Discussion

VEPs were deconvolved by two novel techniques, at frequencies between 10 rps and 25 rps, showing a characteristic shape with no major changes in its form across the subjects but varying according to the stimulus frequency. Main deflections changed in their amplitudes and latencies, with a faster occurrence of the main positive deflection (P1, usually located at 100 ms), observed in the 50 ms to the 100 ms interval as the frequency increases. The negativity (N1, at 135 ms), had the same behavior than the P1, advancing to the 150 ms to the 200 ms interval. For 20 rps and 25 rps, a new positivity occurred, between 150 ms and 200 ms.

VEPs are sensitive to the stimulus nature, and to the VDU used for the stimuli delivery (Odom et al., 2010). In addition, transient VEPs (obtained with the classical averaging process) tend to present differences across subjects, due to the individual characteristics of the visual ways, even in a group of healthy subjects. Aging is also a factor influencing the shape of VEPs, as explained in [17], [18]. During this experiment, such inter-subject differences could be observed in a very coherent fashion; for example, if the subject presented a small amplitude VEPs, those VEPs were small for the entire

set of stimulus rates. No major differences were obtained across the subjects, validating the methods of the deconvolution for the visual potentials.

Other works approached the SSVEPs generation from the individual responses superposition assuming that the shape of the VEP does not change with the stimulus frequency [15], which makes a difference when a synthetic SSVEP is constructed. In addition, the use of CRT displays could affect considerably the acquired signals. As shown in figure 3.6, main frequency components of the SSVEPs can go beyond the 50 Hz and a usual refresh rate of a CRT display could be as low as 24 frame/s.

When analyzing the deconvolved signals for the CLAD and LS methods, some small differences (no statistical significant difference were found) are noted after the first 200 ms. These changes may indicate certain processing due to the nature of the sequences. CLAD signals are obtained from a periodic presentation of stimuli, while LS is composed by a very long non-periodic sequence. Perception of these two types of stimulation may be involved in the resulting signals, as stated in [19], for the auditory system.

The SSVEPs could be "replicated" using the superposition of the individual deconvolved responses. The synthetic SSVEPs are very similar to the acquired SSVEPs, particularly at stimulus frequencies below the 20 rps. At 25 rps, an amplitude difference in the PSD of the signals was observed (see Figure 3.6), however, the linear correlation of the signals in time showed no significant statistical differences for all the experimental conditions. This work showed a synthetic generation using the individual responses obtained by the CLAD method, extending the hypothesis proposed in [16] for the AEPs to the VEPs.

With the time-frequency analysis, a marked difference in the induced activity was observed: theta band and alpha band activities are greater for the low-jittered sequences (both CLAD and LS) than for the isochronic sequences, except in the case of the 10 rps. These results may indicate attentional processes elicited by the jittered nature of the sequences, in agreement with some perception and attention theories [11]. In other words, due to the jitter, the subjects may tend to be more attentive to the stimuli. A deeper assessment must be performed to test the relationship between the jittered sequences and the attention of the subjects.

3.7 References

[1] L. Cao, Z. Ju, J. Li, R. Jian, and C. Jiang, "Sequence detection analysis based on canonical correlation for steady-state visual evoked potential brain computer interfaces," *J. Neurosci. Methods*, vol. 253, pp. 10–17, Sep. 2015.

[2] Yijun Wang, Xiaorong Gao, Bo Hong, Chuan Jia, and Shangkai Gao, "Brain-Computer Interfaces Based on Visual Evoked Potentials," *IEEE Eng. Med. Biol. Mag.*, vol. 27, no. 5, pp. 64–71, Sep. 2008.

[3] J. Bohórquez and Ö. Özdamar, "Signal to noise ratio analysis of maximum length sequence deconvolution of overlapping evoked potentials," *J. Acoust. Soc. Am.*, vol. 119, no. 5, p. 2881, 2006.

[4] F. Bardy, H. Dillon, and B. Van Dun, "Least-squares deconvolution of evoked potentials and sequence optimization for multiple stimuli under low-jitter conditions," *Clin. Neurophysiol.*, vol. 125, no. 4, pp. 727–737, Apr. 2014.

[5] J. Toft-Nielsen, J. Bohorquez, and O. Ozdamar, “Innovative pattern reversal displays for visual electrophysiological studies,” 2011, pp. 2009–2012.
[6] G. H. Klem, H. O. Lüders, H. H. Jasper, and C. Elger, “The ten-twenty electrode system of the International Federation. The International Federation of Clinical Neurophysiology,” *Electroencephalogr. Clin. Neurophysiol. Suppl.*, vol. 52, pp. 3–6, 1999.
[7] J. V. Odom *et al.*, “ISCEV standard for clinical visual evoked potentials (2009 update),” *Doc. Ophthalmol.*, vol. 120, no. 1, pp. 111–119, Feb. 2010.
[8] International Society for Clinical Electrophysiology of Vision *et al.*, “ISCEV standard for clinical visual evoked potentials: (2016 update),” *Doc. Ophthalmol.*, Jul. 2016.
[9] M. R. Nuwer, “Fundamentals of evoked potentials and common clinical applications today,” *Electroencephalogr. Clin. Neurophysiol.*, vol. 106, no. 2, pp. 142–148, Feb. 1998.
[10] S. G. Mallat, *A wavelet tour of signal processing: the sparse way*, 3rd ed. Amsterdam ; Boston: Elsevier/Academic Press, 2009.
[11] J. P. Lachaux, E. Rodriguez, J. Martinerie, and F. J. Varela, “Measuring phase synchrony in brain signals,” *Hum. Brain Mapp.*, vol. 8, no. 4, pp. 194–208, 1999.
[12] E. Maris and R. Oostenveld, “Nonparametric statistical testing of EEG- and MEG-data,” *J. Neurosci. Methods*, vol. 164, no. 1, pp. 177–190, Aug. 2007.
[13] F. Butar and J.-W. Park, “Permutation Tests for Comparing Two Populations,” *J. Math. Sci. Math. Educ.*, vol. 3, no. 2, pp. 19–30, 2008.
[14] J. Bohorquez, S. Lozano, A. Kao, J. Toft-Nielsen, and O. Ozdamar, “Deconvolution and Modeling of Overlapping Visual Evoked Potentials,” 2013, pp. 31–32.
[15] A. Capilla, P. Pazo-Alvarez, A. Darriba, P. Campo, and J. Gross, “Steady-State Visual Evoked Potentials Can Be Explained by Temporal Superposition of Transient Event-Related Responses,” *PLoS ONE*, vol. 6, no. 1, p. e14543, Jan. 2011.
[16] R. E. Delgado and O. Ozdamar, “Deconvolution of evoked responses obtained at high stimulus rates,” *J. Acoust. Soc. Am.*, vol. 115, no. 3, p. 1242, 2004.
[17] M. Kuba, J. Kremláček, J. Langrová, Z. Kubová, J. Szanyi, and F. Vít, “Aging effect in pattern, motion and cognitive visual evoked potentials,” *Vision Res.*, vol. 62, pp. 9–16, Jun. 2012.
[18] G. Stothart, A. Tales, C. Hedge, and N. Kazanina, “Double peaked P1 visual evoked potentials in healthy ageing,” *Clin. Neurophysiol.*, vol. 125, no. 7, pp. 1471–1478, Jul. 2014.
[19] A. Presacco, J. Bohórquez, E. Yavuz, and Ö. Özdamar, “Auditory steady-state responses to 40-Hz click trains: Relationship to middle latency, gamma band and beta band responses studied with deconvolution,” *Clin. Neurophysiol.*, vol. 121, no. 9, pp. 1540–1550, Sep. 2010.

4 EEG Systems

Electroencephalogram (EEG) acquisition systems are widely used as diagnostic and research tools. This chapter shows the implementation of a reconfigurable family of three affordable 8-channels, 24 bits of resolution, EEG acquisition systems intended for a wide variety of research purposes. The three devices offer a modular design and upgradability, permitting changes in the firmware and software. Due to the nature of the Analog Front-End (AFE) used, no high-pass analog filters were implemented, allowing the capture of very low frequency components. Two systems of the family, called “RF-Brain” and “Bluetooth-Brain”, were designed to be light and wireless, planned for experimentation where movement of the subject cannot be restricted. The sample rate in these systems can be configured up to 2000 samples per second (SPS) for the RF-Brain and 250 SPS for the Bluetooth-Brain when the 8 channels are used. If fewer channels are required, the sampling frequency can be higher (up to 4 kSPS or 2 kSPS for 1 channel for RF-Brain and Bluetooth-Brain respectively). The third system, named “USB-Brain”, is a wired device designed for purposes requiring high sampling frequency acquisition and general purpose ports, with sampling rates up to 4 kSPS.

4.1 Introduction

Flexible electroencephalogram (EEG) acquisition systems are required in a wide variety of research fields including brain computer interfaces (BCI) [1], [2], evoked potentials (EPs) [3], [4] stress response[5], [6], epilepsy [3], [7], [8], depth of anesthesia [9]–[11], among others. EEG systems’ extended use is due to its noninvasive nature, high temporal resolution and lower cost compared with other modalities of brain activity monitoring such as functional magnetic resonance imaging (fMRI) or magnetoencephalography (MEG). Also, EEG devices do not require the restriction of the locomotion of the subject under test.

Commercial EEG research systems do not always offer flexibility to configure their settings, such as sampling frequency, location and configuration of the electrodes and individual gain of the channels, among others; and their prices can be high [12], [13]The accessibility to these main features is critical in the experimentation design. Depending on the study, it could be more convenient to have less active channels and a higher sampling rate[14], [15]. Also, the selection of the reference electrode could significantly affect the quality of the acquired data[16]–[18], but changing and testing different locations is time consuming; thus, the possibility of selecting the reference electrode by software, among the electrodes already positioned in the scalp of the subject, would facilitate the assessment of the reference electrode location. The introduction of bias circuits in the EEG systems also improve the acquired signals by reducing the interference of the common-mode and motion artifacts [19]. The function of a bias circuit is equivalent to the right leg drive (RLD) circuits used in ECG systems.

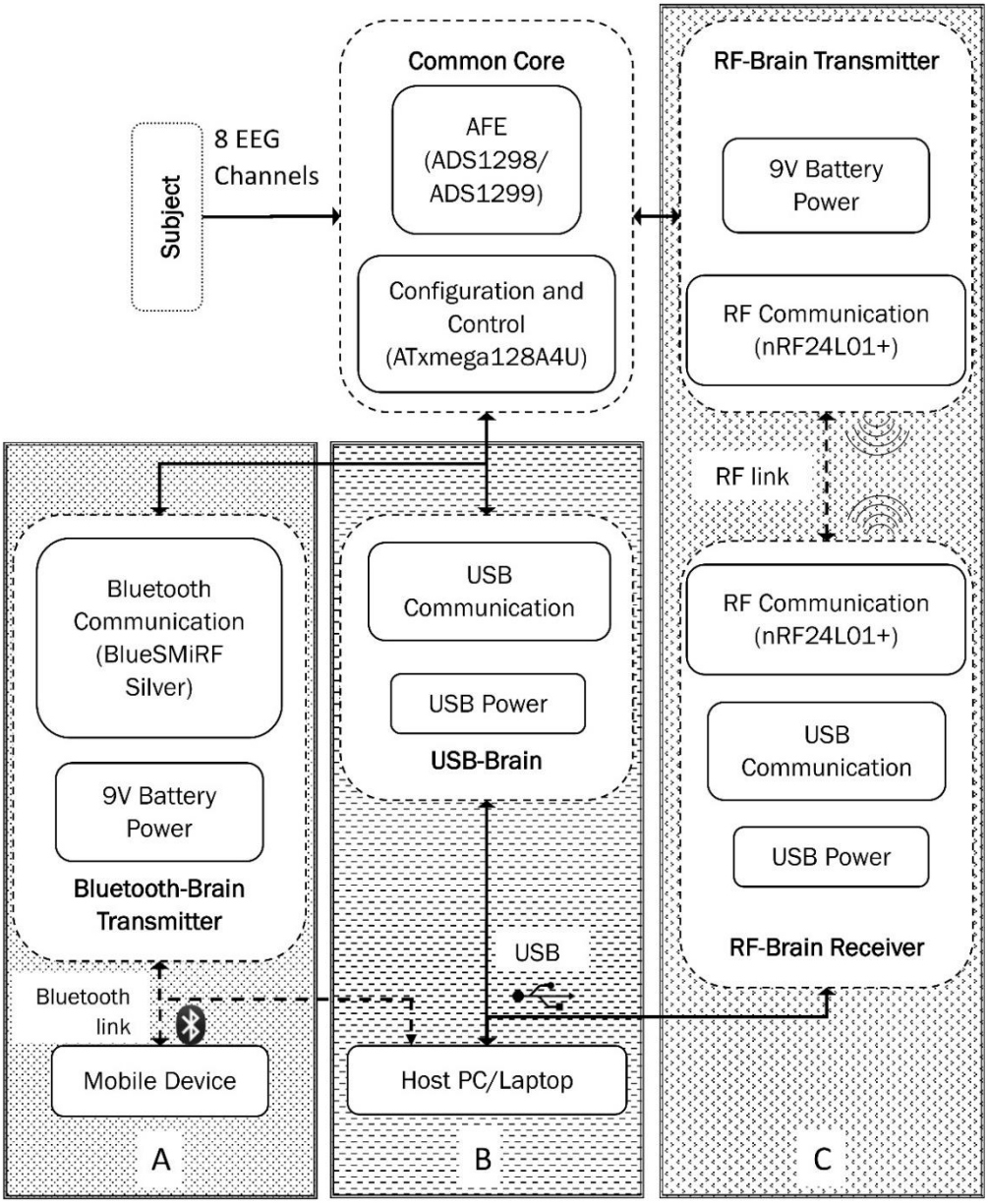

Figure 4.1 Block Diagram of Brain Family. Block diagram of the Brain family of EEG acquisition systems. All devices have a common core composed by the AFE and the control and configuration modules. A. Modules of the Bluetooth-Brain Transmitter can connect to an Android mobile device or to a PC with Bluetooth connectivity. B. Modules composing the USB-Brain, which must be connected directly to a USB port of the host PC. C. Modules for the RF-Brain Transmitter and RF-Brain Receiver. The RF-Brain Receiver connects to a PC through a USB port.

The possibility of selecting the source of the bias signal could result in a better EEG signal. The reconfigurable systems presented here, provide a suitable experimentation tool at a lower cost than commercially available devices, for a broad range of electrophysiological studies. They offer the possibility of changing critical features including sampling rate, number of active channels, individual channel gain and channel input configuration to address the situations mentioned above.

Figure 4.1 presents a block diagram of the family called “the brain family”. Three systems were implemented: RF-Brain, Bluetooth-Brain and USB-Brain. RF-Brain and Bluetooth-Brain are portable, battery-powered devices allowing experimentation where the movement of the subjects is not restricted; for this reason, the size of these systems was kept as small as possible. On the other hand, USB-Brain is powered by the USB port of the host computer where the signals are displayed and/or stored.

All the systems have three main components: hardware for acquisition, firmware that controls the behavior of the systems and a computer or mobile device software for configuration, display and storage of data, through a graphical user interface (GUI). These components were designed in a modular fashion to provide the required flexibility in their settings. Devices are open-hardware and open-software. Through a free-access website (http://ttde.uniandes.edu.co), researchers can retrieve all the necessary information to replicate the systems.

4.2 Main Components of the Brain Family

Table 4.1 Features of the ICs used in the AFE modules[1]

Feature	ADS1299	ADS1298
Analog channels	8	8
Power consumption	5 mW per channel	0.78 mW per channel
Maximum input bias current	300 pA	200 pA
Voltage supply	Analog: 4.75 V to 5.25 V Digital: 1.8 V to 3.6 V	Analog: 2.7 V to 5.25 V Digital: 1.65 V to 3.6 V
Sampling frequency	250 SPS to 16 kSPS	250 SPS to 32 kSPS
CMRR	-110dB	-115dB
Programmable gain	1, 2, 4, 6, 8, 12 or 24	1, 2, 3, 4, 6, 8 or 12
Resolution in Volts	268.22 pV at gain = 1 11.17 pV at gain = 24	143.05 pV at gain = 1 11.92 pV at gain = 12
Resolution in bits	24	24
Input-referred noise	1.62 µVpp (70 Hz of band width at gain = 6)	4 µVpp (150 Hz of band width at gain = 6)

4.2.1 Core

All designed systems share a common core (see Figure 4.1) composed by two modules: analog front-end (AFE) and configuration and control.

[1]Values taken from the ICs datasheets available at www.ti.com

4.2.1.1 AFE

Depending on the system, the AFE module may use one of the following integrated circuits (ICs) from Texas Instruments®: ADS1298 or ADS1299.

Both ICs have eight channels with an instrumentation programmable gain amplifier (PGA) each one and 24 bit sigma-delta analog-to-digital converter (ADC). PGAs offer a set of possible gains from 1 to 24. The resolution in bits of the ADC, along with these set of gains provide an approximately resolution of 12 pV. For 16 bit systems, the required gain to achieve the same resolution would have to be in the order of 103. AFEs maximum input bias current is 200 pA and 300 pA for the ADS1298 and the ADS1299 respectively. These ICs have an input multiplexer per channel for device noise measurement, test signal generation and acquisition, temperature measurement and supply voltage measurement. Main features of the two ICs are listed in

Table 4.1.

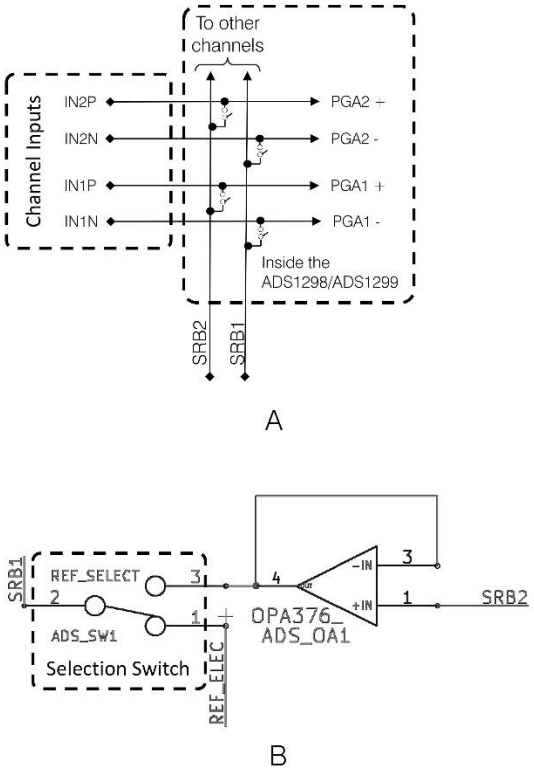

Figure 4.2 Circuit and internal diagram of the variable reference circuit. A. Internal diagram of the ADS 1299 or ADS1298. SRB2 can be connected to any individual positive channel input and SRB1 can be connected to all negative channel inputs. B. When using single

The ADS1298 was used in the RF-Brain and Bluetooth-Brain as it offers a lower power consumption and a bigger supply voltage range (see

Table 4.1), reducing the complexity of the energy module and therefore the space required in the printed circuit board (PCB). These features are desired for portable devices in order to offer more

autonomy and less space and weight. Since the USB-Brain takes the energy from the USB port, the restriction in power consumption is not relevant, for that reason the ADS1299 was used, offering a better input-referred noise and a bigger gain (up to 24, see

Table 4.1).

In all systems, the individual channel gain and the behavior of the input multiplexer can be selected from the user interface or modified by firmware. These settings are sent to the configuration and control module and are established at the beginning of the acquisition process.

In the Bluetooth-Brain system, all channels are single-ended, referred to a fixed electrode called reference electrode which also serves as bias electrode. The RF-Brain also has single-ended channels, but it offers the option of selecting the reference electrode between an independent electrode and one of the channel electrodes; these settings are selected through the GUI and an analog switch located on the board of the system, as shown in Figure 4.2. With the analog switch, the user can select to connect all negative inputs to the reference electrode or to the pin called SRB2, which can be selected among any electrode connected to the positive input of the AFE. The bias signal can also be configured with the help of a switch and the user interface.

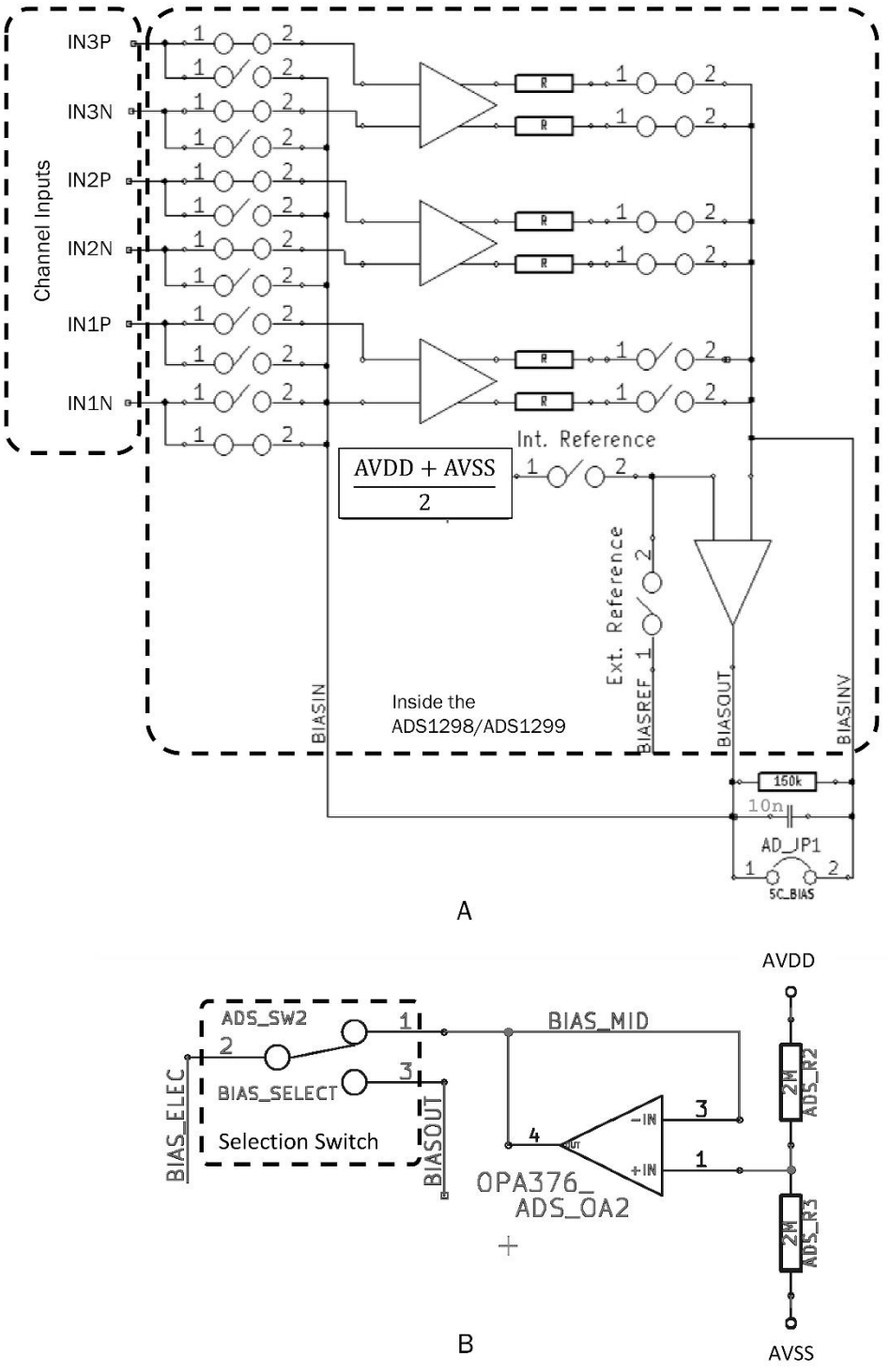

Figure 4.3 Bias signal circuit and internal diagram. A. Internal diagram of the ADS1299 or ADS1298. Channels can be selected for the bias derivation in the GUI or firmware. In this figure, channels 2 and 3 generate the bias signal, which is then routed to the negative input of channel 1. B. User can choose the bias signal origin between the generated from the internal circuitry of the IC or the one at output of the operational amplifier which is the mid-supply voltage.

Figure 4.3 shows the internal and external diagram of this implementation. Bias signal may be formed from a set of electrodes selected by the user from the GUI and can be connected to the subject with the bias electrode. Its purpose is to reduce the common-mode interference by creating a negative feedback loop to the subject, equivalent to the RLD signal in ECG systems. If this is not required, the user can select the bias signal to be the mid-supply voltage. The external electronics explained above were designed based on the ADS1299EEG-FE performance demonstration kit, the information of which is available online in www.ti.com.

In the case of the USB-Brain system, the user can configure the channels to be differential or single-ended. In the single-ended configuration, the reference and the bias signal can be set in the same way as for the RF-Brain (Figure 4.2 y Figure 4.3).

No analog high-pass filters were implemented, allowing capture of signals from DC and avoiding possible distortions due to the nonlinearities of the analog filters. Systems were designed to be used with floating type, cup electrodes with 1.5 mm touch proof connector (DIN 42 802) [20].

4.2.1.2 Configuration and Control

The configuration and control module consists of a high performance, low power, 8-bit microcontroller from Atmel® (ATxmega128A4U). It receives the orders from the user and sets the configuration of the other modules. It also works as a buffer for the data, between the AFE and the communication modules. The microcontroller works at 32 MHz, and can perform simple processing of the data. The communication with the other modules is done through serial peripheral interfaces (SPI), whose baud rate can be modified in the firmware between 1 M bits per second (bps) to 10 Mbps.

The general processes made by this module are shown in the flow diagram of Figure 4.4. For RF-Brain and USB-Brain systems the microcontroller is in sleep mode at the beginning and all the other modules are off to save energy. After an “on-signal” is sent from the user, microcontroller wakes up and turns on all the other modules. The configuration parameters (like sampling frequency, gain and input multiplexer) are sent from the host PC. In the case of the Bluetooth-Brain system, the microcontroller is on and the Bluetooth transceiver is in discovery mode or connected to the receiver at the beginning. Settings must be configured in the microcontroller firmware by using a programmer device for the microcontroller and a software to load the code (for example the Atmel® Studio). Firmware of all systems was written in C and can be updated using the program and debug interface (PDI) port available in all the devices.

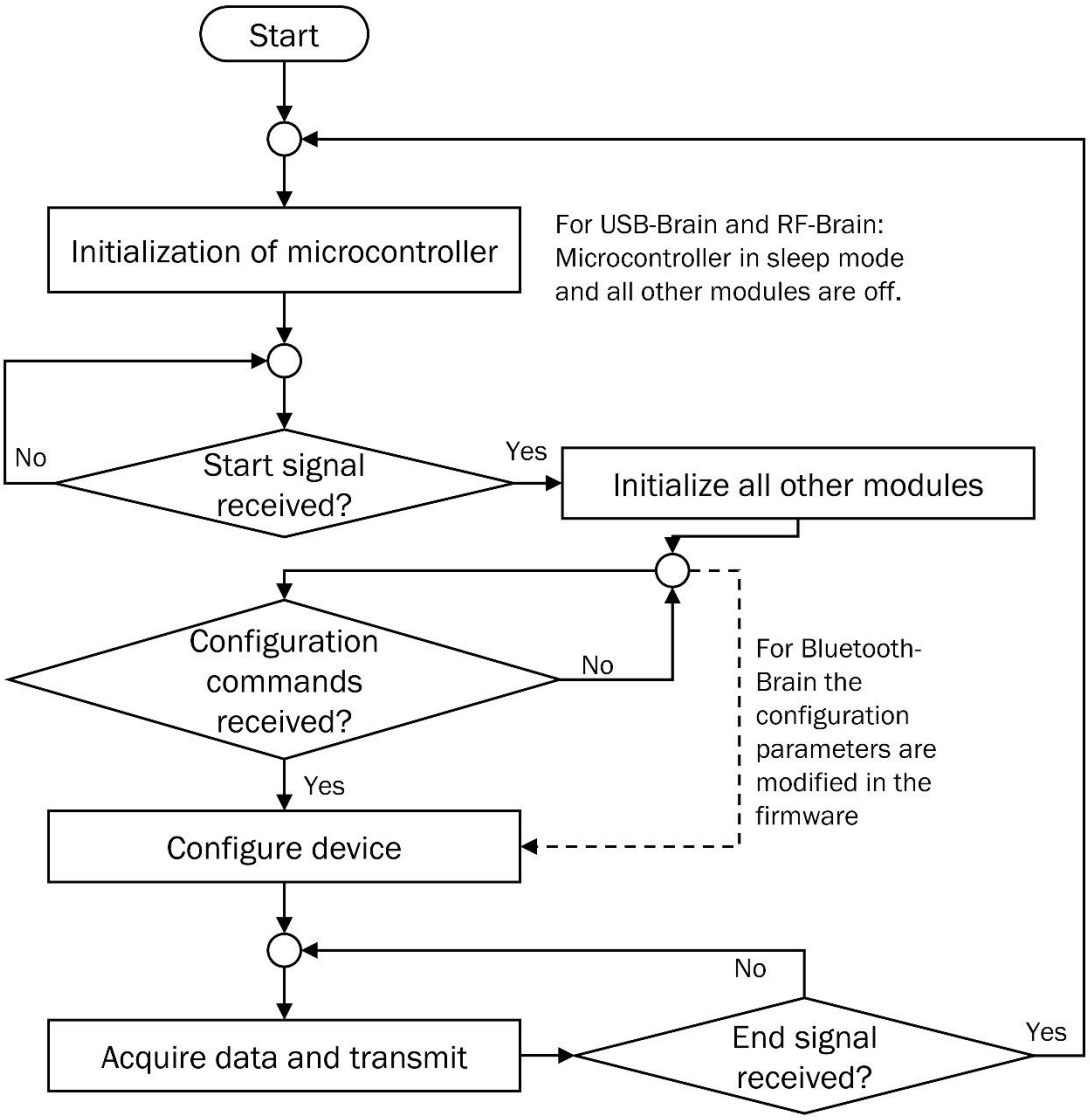

Figure 4.4. Flow diagram of the main processes in the configuration and control module.

4.2.2 RF-Brain

The first system of the family is formed by two boards: the first, a small and light transmitter is suitable for biofeedback and BCI applications, and is in charge of the acquisition, digitalization and transmission of data; the second, a USB receiver, is connected to a host computer for display, storage and processing of the signals. This device is an updated version of the Wireless Neuro Boards presented in [21], improving 60 Hz/50 Hz noise isolation and providing more flexibility for the electrode configuration. Improvements were done by modifying all the connectors of the transmitter board and adding some components for the selection of reference and bias electrode, as explained in the previous section.

4.2.2.1 Transmitter

The transmitter is a battery powered device formed by four modules: configuration and control, AFE, wireless RF communication and energy.

For the communication, an RF transceiver from Nordic Semiconductor® was used (nRF24L01+). It operates at the industrial scientific and medical (ISM) band of 2.4 GHz and is capable of reaching an on-air data rate of 2 Mbps, limiting the sampling frequency of the AFE which can be configured up to 2 k samples per second (SPS), when all channels are active. If only one channel is active, the sampling frequency can be selected up to 4 kSPS.

The energy module generates a regulated 3.3 V required for all the other components in the board, from a standard 9 V battery. The maximum current consumption was estimated as 30.21mA at a sampling frequency of 250 SPS, when all channels are active at programmable gain of 12; providing a battery life of more than 18 hours when using an alkaline battery of 550 mAh.

The device is a board approximately 60 mm long, 38mm wide and 10 mm high. The weight of the transmitter is approximately 10 g without the 9 V alkaline battery whose weight is around 45 g. Its weight makes this device appropriate for humans and animals of 500 g or more.

4.2.2.2 Receiver

In this device, control and configuration and RF-Communication modules are formed by the same components used for the transmitter. The USB communication module has a FTDI® FT232H IC, which is a converter from serial/parallel to Hi-speed USB, allowing transfer of data at baud rates from 115.2 kbps to 1.38 Mbps. The receiver is powered from the USB port of the host computer, with an energy module to offer regulated 3.3V to all the other modules.

4.2.3 Bluetooth-Brain

Based on the architecture of the RF-Brain system, this portable device was designed to easily connect with smartphones and tablets through a Bluetooth modem (BlueSMiRF Silver from SparkFun Electronics®). This modem is capable of transmitting data at a serial stream of 115200 bps, permitting the system to record EEG signals at 250 SPS. As shown in Figure 4.1, the other modules are similar to those in the RF-Brain. When using a 9 V alkaline battery of 550 mAh, the system may work continuously for approximately 7 hours (8 channels active with programmable gain of 12). It is required for the receiver device to have Bluetooth connectivity (Bluetooth v2.0 or higher). Some embedded devices need a Bluetooth dongle to achieve this connectivity. For storage, visualization and processing of data, a GUI for Android devices was specially designed. MATLAB® GUI was also designed for the cases where the receiver is a Windows® laptop or PC. Basic functions are available: selection of channels of acquisition, visualization of signals and storage options.

4.2.4 USB-Brain

This system was designed for experimentation where high sampling frequency is required and offers more options for electrode configuration and external hardware synchronization. Communication is made directly through the USB port of the host PC using a FTDI® serial/parallel to USB converter.

Since the data do not need to be wirelessly transmitted, the sampling frequency can be set from 250 SPS to 4 kSPS.

The processing module uses the ATxmega128A4U microcontroller from Atmel® and a 32 KB SRAM chip was integrated for loading of files (for example, stimulation sequences when used to acquire evoked potentials) into the system. 8 general purpose input/output pins are available and can be used for different tasks such as synchronization with external hardware (for example, stimuli delivery) or interactions with the subject during the tests.

USB-Brain is powered through the USB port of the host computer. The power module delivers three voltage levels from the 5 V of a standard USB port: ± 2.5 V for the AFE and other analog modules, and 3.3 V for all the digital components. It also provides an isolation of 3 kVDC from a DC/DC converter (Texas Instruments® DCH010505D) to ensure the safety of the subject under test. Transfer of data is also isolated through a digital coupler (Texas Instruments® ISO150) to avoid any current flow from the PC or laptop to the subject.

Total current consumption of the system during normal operation is approximately 117 mA at a sampling frequency of 250 SPS and a channel programmable gain of 12, with all channels active in differential mode. The dimensions of the main board of the system are: 91 mm wide by 112 mm long by 10 mm height, and its weight is 100 g.

4.2.5 Configuration and Acquisition Interfaces

GUIs were implemented in MATLAB® for all the systems in the family when using a PC or laptop. From the GUIs, the user can select the channel configuration, sampling frequency and the options of storage and visualization of the data. The options vary depending on the system. Figure 4.5 shows the GUI for the USB-Brain system.

Table 4.2 Features of the Brain family of systems.

Option	RF-Brain	Bluetooth-Brain[2a]	USB-Brain
EEG channels	8	8	8
Receiver baud rate	115200 bps to 921600 bps	115200 bps	115200 bps to 921600 bps
Individual channel gain	Off, 1, 2, 3, 4, 6, 8 or 12	Off, 1, 2, 3, 4, 6, 8 or 12	Off, 1, 2, 4, 6, 8, 12 or 24
Input configuration	Shorted, test signal, normal	Shorted, test signal, normal	Shorted, test signal, normal
Sampling frequency	8 channels: 250 SPS to 2 kSPS 1 channel: 250 SPS to 4 kSPS	8 channels: 250 SPS 1 channel: 250 SPS to 2 kSPS	250 SPS to 4 kSPS

[2] For Bluetooth-Brain, the options can be selected by changing the firmware, not by the GUI.

Reference	Reference electrode or any channel electrode[b]	Bias/reference electrode	In single-ended mode: Reference electrode or any channel electrode[3b]
Bias	Bias electrode, any channel electrode or internally generated bias[c]	Bias/reference electrode	Bias electrode, any channel electrode or internally generated bias[4c]
Maximum power consumption inactive[5d]	2.64 mA	66.7 mA	77.7 mA
Maximum power consumption active[6e]	30.21 mA	76.7 mA	117.1 mA
Data error in transmission for a range of 5 m	0 bits	0 bits	NA
Data loss in transmission for a range of 5 m	0 packages	0 packages	NA

For the RF-Brain and USB-Brain, in the current GUIs, the following options are available:

- Short Circuit: All inputs shorted. For the RF-Brain all inputs connected internally to the reference electrode. For the USB-Brain, the inputs are connected either positive input with negative input or positive input to reference electrode, depending on the electrode configuration. These settings provide a way to measure noise levels in the system.
- Test Signal: When activated, an auto-generated square signal from the AFE, with amplitude of 1 mV and a frequency of 1 Hz approximately, is generated and helps to verify the correct acquisition and communication link in the case of the RF-Brain.
- Normal: The normal operation of the channels for EEG acquisition.

[3] External switch must be set according to the reference selection (see Figure 4.2)
[4] External switch must be set according to the bias selection (see Figure 4.3)
[5] For RF-Brain and USB-Brain, microcontroller in sleep mode and all other modules off. For the Bluetooth-Brain, Bluetooth device in discovery mode.
[66]All channels active in normal operation, gain of 12 and sampling frequency of 250 SPS

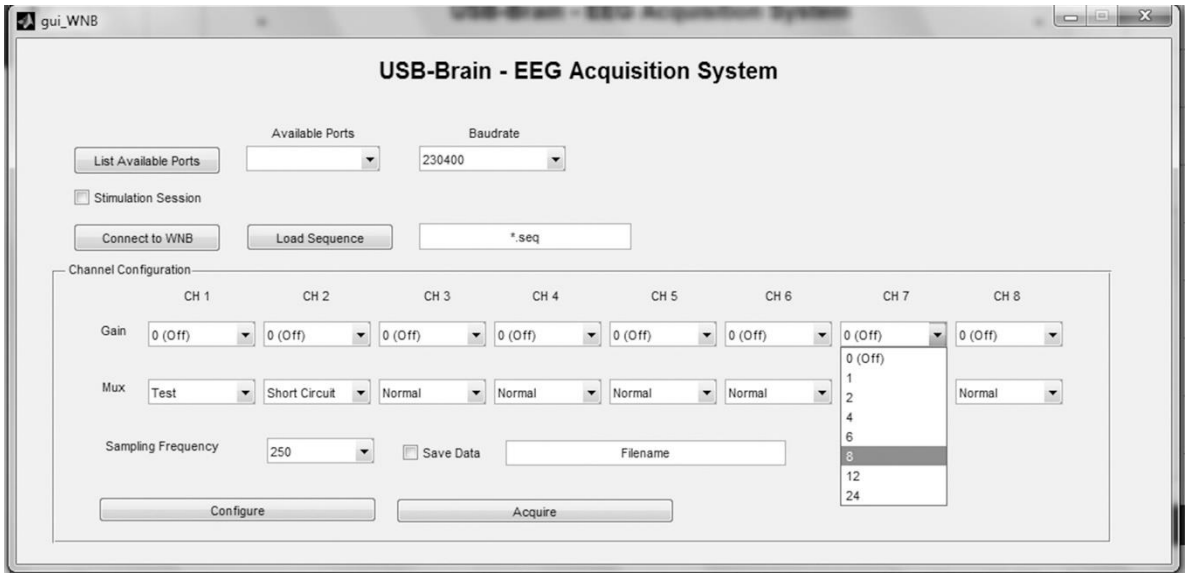

Figure 4.5. GUI for the USB-Brain.User can choose the main features of the system to accomplish the requirements of the experiment.

For Bluetooth-Brain, these options can be modified from the firmware of the system. Table 4.2 shows the available options for all the devices. Additionally, for the Bluetooth-Brain, an Android GUI was designed where the user can select channels to visualize the data and store the signals into a file for further off-line processing.

4.2.6 Modularity

All systems were designed to be modular with the purpose of making changes easily when the experimentation requires it. For this reason, it was possible to make a whole family of systems by changing some modules in the design. Other possible modifications from the core of the family may include, for instance, the addition of more AFEs to increase the channel number, through a daisy-chain connection, avoiding the use of more pins in the microcontroller; for this modification the SPI communication baud rate and the sample rate must be taken into account: for a sample rate of 1 kSPS and a SPI communication at 1 MHz, 5 AFEs (with 8 channels each one) can be daisy-chained for a total number of 40 channels.

The communication module can be replaced in all systems, for example when other type of communication is required (wired or wireless). As long as an SPI communication protocol can be used, no major changes must be done in the firmware of the devices.

When access to firmware is required, a PDI port is available in all the systems to change the firmware of the microcontroller and the basic configuration of the AFE.

4.3 Performance Assessment of Brain Family

All systems have different features; Table 4.2 summarizes the main characteristics of the family. The following aspects were tested for each system: power consumption, communication reliability (for the case of wireless devices) at all possible sampling rates, electric noise and acquisition of test

signals. Pilot tests were done with human subjects to record EEG signals. During the tests, the environment was not controlled, meaning that Wi-Fi signals and mobile cell phones were present in the area of tests.

4.3.1 Power Consumption

Power consumption was measured in all systems at standby and regular operation. The standby condition implies, for the RF-Brain and the USB-Brain, that the microcontroller is in sleep mode and all the other modules are off. For this condition, maximum power consumption of the devices was 2.64 mA and 77.7 mA for the RF-Brain and the USB-Brain respectively. Power module and extra components in the USB-Brain system are responsible for its higher current consumption compared to the RF-Brain. In the case of the Bluetooth-Brain, the standby conditions mean that the microcontroller is on and the Bluetooth transceiver is either in discovery mode or connected to the receiver device, but no data is transmitted. Its current consumption is 66.7 mA.

In the case of regular operation, all channels in the systems were active in normal configuration, with a gain of 12 and a sampling frequency of 250SPS. For the RF-Brain, the maximum power consumption was 30.21 mA; the Bluetooth-Brain has a maximum power consumption of 76.7 mA and the USB-Brain consumes at most 117.1 mA.

4.3.2 Communication range and reliability

To test the communication range and reliability, a periodic saw-tooth signal was synthetically generated in the microcontroller and sent to the host computer or receiver for a minimum period of 10 minutes. All systems were tested at the complete set of the sampling frequencies. USB-Brain system communication did not present any data corruption or loss for all the sampling frequencies. Tests were also performed for the two wireless systems, changing the distance between the receiver and the transmitter. No data loss or corruption was presented for a distance of 5 m or less from the receiver.

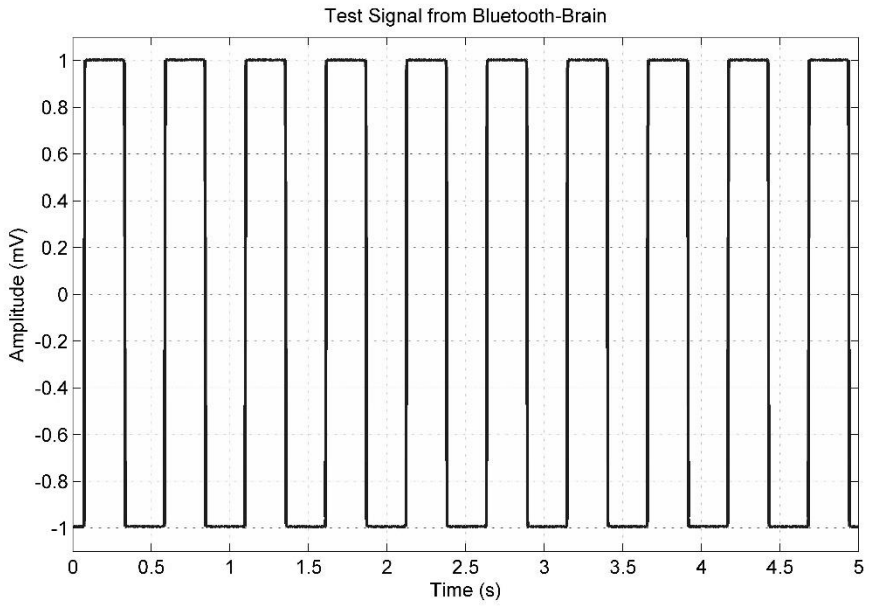

Figure 4.6 Test signal acquired with the Bluetooth-Brain. Test signal is internally generated by the IC in the AFE module and consists on a squared wave of 1mV of amplitude and 1Hz of frequency.

4.3.3 Noise Measurement

A noise test took place for a set of sampling frequencies. The test consisted of shorting the inputs of the amplifiers through the input multiplexer settings and acquiring the signals. Noise measurements were made for 1000 continuous readings. Average results of all channels are detailed in table 4.3.

Table 4.3 Input referred noise measurements for the systems[a]

Sampling Frequency	RF-Brain		Bluetooth-Brain		USB-Brain	
	µVrms	µVpp	µVrms	µVpp	µVrms	µVpp
250 SPS	0.49	2.20	0.50	4.16	0.16	1.13
500 SPS	0.52	3.25	NA	NA	0.23	1.61
1 kSPS	0.72	4.44	NA	NA	0.32	2.26
2 kSPS	0.91	6.56	NA	NA	0.46	3.20
4 kSPS	NA	NA	NA	NA	0.65	4.53

[a] Gain was set at 12 for all systems.

4.3.4 Test Signal

To assess the integrity of the PGAs, its adequate calibration and visualization capability of the graphic interface, a test signal was acquired through all the channels of the three systems, at different gain settings. The test signal is an internally generated (generated inside the AFE ICs), square wave of 1 mV of amplitude and 1 Hz of frequency. An example of the acquired test signal is shown in Figure 4.6

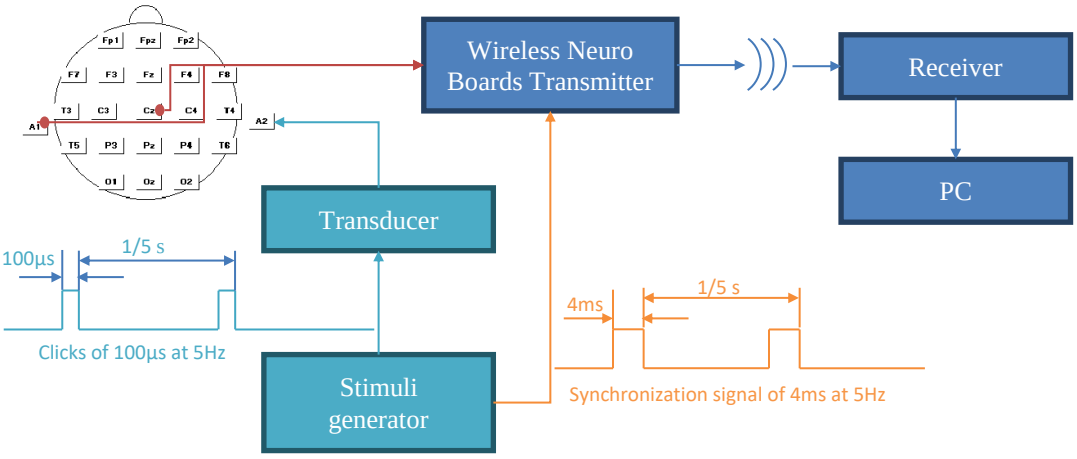

Figure 4.7 Block diagram for the AEP Test.Along with the RF Brain system, an auditory stimuli generator was used. Red arrows represent the electrophysiological signals, aquamarine arrows represent the auditory signals, orange arrow is the digital synchronization signal and blue arrows represent the data transmission through the acquisition system

4.3.5 Pilot Tests

To evaluate the quality of the acquired physiological signals, a variety of tests were made for each system. All physiological signals were acquired from healthy human subjects who gave consent for the use of the data. Electrode location follows the standard ten-twenty electrode system [14], [22]. All procedures explained in this section were approved by the Research Ethical Committee of Universidad de los Andes – Bogotá – Colombia, or the Institutional Review Board of the University of Miami – Florida – United States, in fulfillment of the Code of Ethics of the World Medical Association. The following tests were done:

RF-Brain: auditory evoked potentials (AEPs) were acquired with the RF-Brain system from one subject (S1, 27 years old) using a data rate of 500 SPS and a gain of 12 in the PGAs. The experimental setup consisted on an electrode located in Cz and referred to A1 for ipsilateral acquisition. Bias signal was selected at mid-supply voltage and located also at A1. The stimulus used was monaural rarefaction clicks at 60 dB nHL at a frequency of 6 stimuli per second. Etymotic Research ER3 insert earphones were used. Figure 4.7 shows the setup.

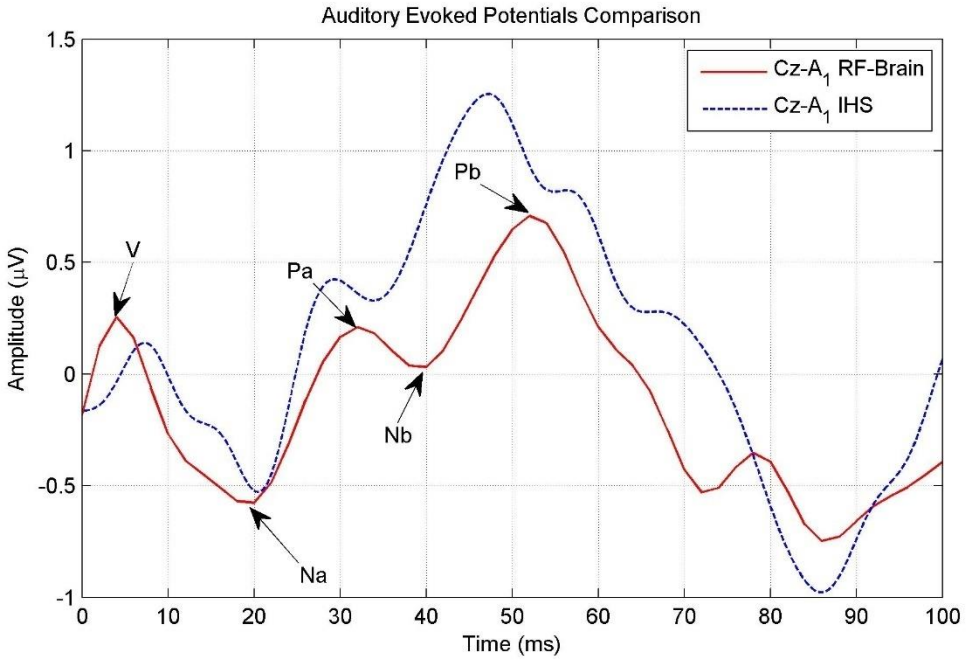

Figure 4.8 Auditory evoked potentials acquired with RF-Brain system and the IHS Universal Smart Box.720 sweeps were averaged to obtain the evoked potentials. Main waves of a typical AEP are observed and marked as "Na", "Pa", "Nb" and "Pb". A small difference in the amplitude can be observed, but latencies and morphology of the signals are similar

We wanted to assess the performance of the RF-Brain by comparing the signals acquired against signals from a commercial system; for this purpose we used the Intelligent Hearing Systems (IHS) Universal Smart Box at a sampling frequency of 500 SPS and a gain of 100000 (high-pass filter at 1Hz and low-pass filter at 1500 Hz). A total of 720 sweeps were recorded and averaged to extract the evoked potential. Figure 4.8 shows the results for the RF-Brain and the commercial system. The typical shape of an AEP (middle latency response) can be observed: two positive waves (marked as Pa and Pb), and two negative waves (Na and Nb) [23]. A difference in the amplitude of the signals is observed and may be due to the use of filters in the IHS system. Latencies and morphology of the signals are similar, taking into account the number of sweeps used for the computation of the potentials (see [3]).

Additionally, EEG signals were registered from another subject (S2, male 27 years old), with one electrode located at Oz and referred to Fpz. Sampling rates of 500 SPS and 1 kSPS were used at a gain of 12. Alpha waves were observed for the periods of time where the subject had his eyes closed [20].

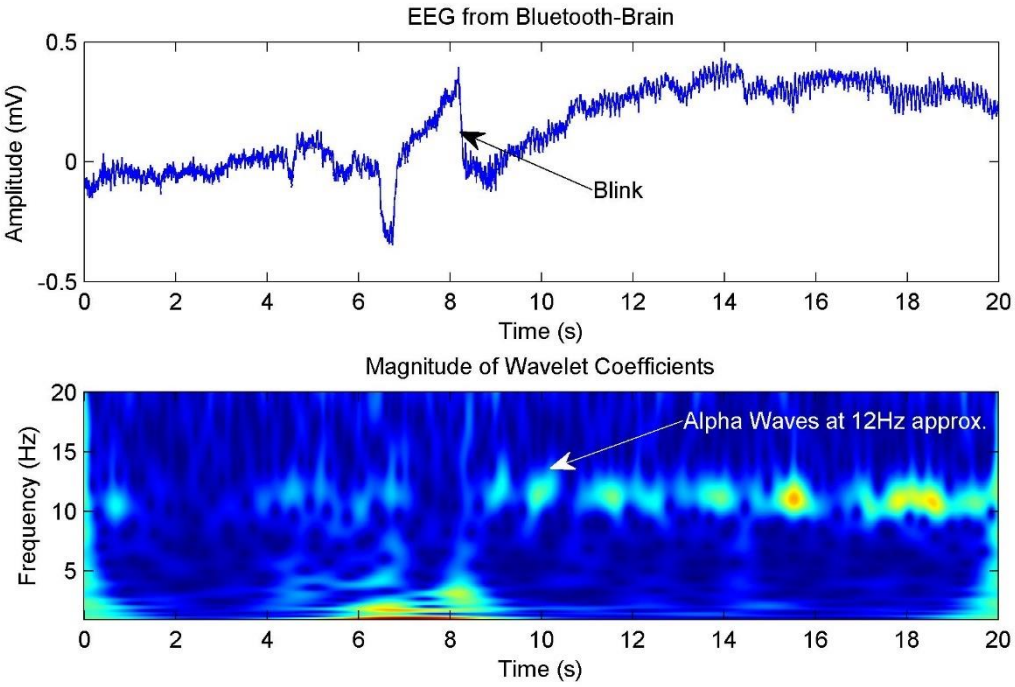

Figure 4.9 EEG signal acquired with the Bluetooth-Brain for subject S3 along with its time-frequency spectrogram to show its main frequency components. Electrodes were located in Oz with reference and bias in Fpz. Alpha waves (at 10 Hz approximately) can be observed after the subject closes his eyes.

Bluetooth-Brain and USB-Brain: Following a similar procedure than for the RF-Brain, EEG signals were acquired with the Bluetooth-Brain and the USB-Brain, from two human subjects (S3, male, 22 years old and S4, male, 29 years old) using an electrode in Oz referred to Fpz, for a sampling rate of 250 SPS and a gain of 12 in the case of the Bluetooth-Brain. For the USB-Brain, sampling frequencies of 2 kSPS and 4 kSPS were used for a gain of 24 in the PGAs. An example of these acquired signals is shown in figure 4.9, where a time-frequency representation is also depicted to view main frequency components. Alpha waves can be observed when the subject closes his eyes at approximately 10 Hz.

4.4 Discussion

Three modular, flexible, affordable and high-performance systems were described in detail in this chapter. All members of the family of systems have a common core composed by an AFE and a control and configuration module. Two wireless systems were designed for BCI and biofeedback applications where movement of the subjects is not restricted: RF-Brain and Bluetooth-Brain. Since these two systems are battery powered instead of being connected to the line power, the safety of the subject under test is assured. Bluetooth-Brain offers the possibility of connecting the system to a mobile device like a tablet or smart-phone. The third, a wired system, offers options for experimentation where high sampling rates, synchronization and general purpose ports are needed. Flexibility is the result of the modular and open nature of the devices, which allows the selection of main features through GUIs and firmware upgrades for the control and configuration module. A

website was created to document and provide access to all systems information, including schematics and C code of the microcontroller: ttde.uniandes.edu.co\.

A variety of tests were made to assess the performance of the family, including power consumption, range and integrity of communication link, synthetic signals and a pilot test with electrophysiological signals. Results have been positive, showing a performance similar or better to other systems like the ones presented in [24]–[27]. A comparison between the Brain family and other systems is shown in table 4.4.

Table 4.4 Comparison of the systems against other similar devices.

Feature	**Value**					
	Brain Family (RF / Bluetooth / USB)	**Brown et al. 2010 [3]**	**Chi et al 2013 [4]**	**Lin CT et al 2014 [16] Mindo-4**	**Emotiv EPOC[a]**	**ABM B-Alert X10[b]**
Channels	8	8	32	4	14	9
Type of electrode	Passive	Active	Active	Passive	Passive	Passive
Electrode connection	Gel	Direct	Direct	Direct	Saline-infused felt	Gel-infused foam
Sampling frequencies (SPS)	250 to 4000[c]	500 or 1000	250	128 to 512	128	256
ADC resolution (bits)	24	11	24	24	14	16
Transfer	RF / Bluetooth / USB	RF	Bluetooth	RF	RF	Bluetooth
Supply voltage (V)	9 / 9 / 5	-	-	-	-	3.7
Supply current (mA)	30.21 / 76.7 / 117.1	4.3 approx.	-	-	-	40 approx.
Battery life (hours)	18 / 7 / -	30	5 approx.	23	>12	>8
Input referred	0.49[d] / 0.50[d] / 0.16[d]	-	1	-	-	2 approx.

noise (µVrms)						
CMRR (dB)	115 / 115 / 110	-	100	-	85 approx.	105
Price (USD)	450[e]	-	-	-	700[f]	9950

[a] *System from Emotiv Inc. Information retrieved from the manufacturer website: https://emotiv.com/epoc.php*

[b] *System from Advanced Brain Monitoring Inc. Information retrieved from the manufacturer website: http://www.advancedbrainmonitoring.com/*

[c] *Depending on the specific system and the number of acquisition channels (see table 2).*

[d] *For normal operation, 8 channels on, gain of 12 and sampling frequency of 250 SPS.*

[e] *Rough price per system including electronic components and PCB manufacturing.*

[f] *Price of the product including access to raw EEG signal*

Although some commercial systems, like Cognionics 32-channel headset, have a greater number of channels [25], brain family has a higher sampling frequency and the same bit resolution. In fact, compared with any other system listed in table 4.4, brain family devices may be set at a higher sampling frequency. Another aspect to mention is their autonomy: while other systems are capable of working continuously for up to 5 hours, brain family systems can work for more than 18 hours with a standard 9V alkaline battery.

Costs of manufacturing the systems are lower than the price of devices like the Emotiv Epoc (https://emotiv.com/epoc.php) or the ABM B-Alert X10 (http://www.advancedbrainmonitoring.com/), accomplishing one of the main goals of the implementation of the brain family, which was to offer high performance devices at a lower price.

One factor to be accounted for the brain family systems is the electrode positioning, which must be done manually with wet electrodes. This may require more time at the beginning of experimentation than when using other devices for which the electrodes are located in a structure with pre-defined locations. However, some locations or structures of electrodes are not suitable for all head sizes and for the cases where dry electrodes are used, the pressure required for the fixation of the sensors generates discomfort in the subjects [13]. This is avoided with the gel electrodes. Also, the lack of a pre-defined structure allows the adaptation for any head size or the use of non-standard locations of electrodes.

4.5 Conclusion

A group of affordable and flexible EEG acquisition systems was described in detail in this section. To assess the performance of the devices, a variety of tests took place. The results for all systems with synthetic test signals and electrophysiological signals showed that the devices are suitable tools for research areas involving EEG signals.

The cost of the devices (less than 500 USD each one) marks an important advantage over commercial systems. However, the manufacturing process may be time consuming and require a

thorough knowledge of electronics. For the wireless devices, further improvements in the systems may include the use of an internal and rechargeable battery, even though the use of an external, alkaline battery provides enough autonomy for most of the experiments.

Modularity of the systems enables the researcher to independently manage the acquisition, processing and transmission of the signals to a host computer. This fragmentation allows the researcher to make decisions about the settings required, in accordance with the restrictions imposed by the experimentation protocol in relation to the mobility of the subject, sampling frequency, gain and configuration of the electrodes. As a future project, with further modifications to the core of the devices, the authors want to provide a main board to which daughter boards can be attached, depending on the specific requirements of the experimentation in communication mode (wireless or wired), availability of synchronization ports, general purpose inputs or outputs and memory modules, among others.

4.6 References

[1] B. J. Kim, M.-H. Lee, and S.-W. Lee, “Intention analysis based on brain signal for participation induction during rehabilitation,” 2015, pp. 1–2.

[2] G. R. Naik and Y. Guo, Eds., *Emerging Theory and Practice in Neuroprosthetics:* IGI Global, 2014.

[3] J. T. Valderrama, A. de la Torre, I. Alvarez, J. C. Segura, M. Sainz, and J. L. Vargas, “A flexible and inexpensive high-performance auditory evoked response recording system appropriate for research purposes,” *Biomed. Eng. Biomed. Tech.*, vol. 59, no. 5, Jan. 2014.

[4] E. Yin, Z. Zhou, J. Jiang, Y. Yu, and D. Hu, “A Dynamically Optimized SSVEP Brain–Computer Interface (BCI) Speller,” *IEEE Trans. Biomed. Eng.*, vol. 62, no. 6, pp. 1447–1456, Jun. 2015.

[5] T. S. Mel’nikova, S. I. Andrushkyavichus, and V. N. Krasnov, “Diurnal Dynamics of Reactivity in a Stress Test in Patients with Depression,” *Neurosci. Behav. Physiol.*, vol. 45, no. 4, pp. 398–403, May 2015.

[6] T. Meyer *et al.*, “The role of frontal EEG asymmetry in post-traumatic stress disorder,” *Biol. Psychol.*, vol. 108, pp. 62–77, May 2015.

[7] S. F. Azab *et al.*, “Childhood temporal lobe epilepsy: correlation between electroencephalography and magnetic resonance spectroscopy: a case–control study,” *Ital. J. Pediatr.*, vol. 41, no. 1, Dec. 2015.

[8] I. Mporas, V. Tsirka, E. I. Zacharaki, M. Koutroumanidis, M. Richardson, and V. Megalooikonomou, “Seizure detection using EEG and ECG signals for computer-based monitoring, analysis and management of epileptic patients,” *Expert Syst. Appl.*, vol. 42, no. 6, pp. 3227–3233, Apr. 2015.

[9] I. Constant and N. Sabourdin, “Monitoring depth of anesthesia: from consciousness to nociception. A window on subcortical brain activity,” *Pediatr. Anesth.*, vol. 25, no. 1, pp. 73–82, Jan. 2015.

[10] Z. Liang *et al.*, “EEG entropy measures in anesthesia,” *Front. Comput. Neurosci.*, vol. 9, Feb. 2015.

[11] M. Peker, B. Şen, and H. Gürüler, “Rapid Automated Classification of Anesthetic Depth Levels using GPU Based Parallelization of Neural Networks,” *J. Med. Syst.*, vol. 39, no. 2, Feb. 2015.

[12] V. Mihajlovic, B. Grundlehner, R. Vullers, and J. Penders, “Wearable, Wireless EEG Solutions in Daily Life Applications: What are we Missing?,” *IEEE J. Biomed. Health Inform.*, vol. 19, no. 1, pp. 6–21, Jan. 2015.

[13] W. David Hairston *et al.*, “Usability of four commercially-oriented EEG systems,” *J. Neural Eng.*, vol. 11, no. 4, p. 046018, Aug. 2014.
[14] K. Kobayashi *et al.*, “Detection of seizure-associated high-frequency oscillations above 500Hz,” *Epilepsy Res.*, vol. 88, no. 2–3, pp. 139–144, Feb. 2010.
[15] Y. Iwatani *et al.*, “Ictal high-frequency oscillations on scalp EEG recordings in symptomatic West syndrome,” *Epilepsy Res.*, vol. 102, no. 1–2, pp. 60–70, Nov. 2012.
[16] S. H. Choi, M. Lee, Y. Wang, and B. Hong, “Estimation of Optimal Location of EEG Reference Electrode for Motor Imagery Based BCI Using fMRI,” 2006, pp. 1193–1196.
[17] A. K. O. Paukkunen and R. Sepponen, “The effect of ground electrode on the sensitivity, symmetricity and technical feasibility of scalp EEG recordings,” *Med. Biol. Eng. Comput.*, vol. 46, no. 9, pp. 933–938, Sep. 2008.
[18] W. Speier, A. Deshpande, and N. Pouratian, “A method for optimizing EEG electrode number and configuration for signal acquisition in P300 speller systems,” *Clin. Neurophysiol.*, vol. 126, no. 6, pp. 1171–1177, Jun. 2015.
[19] A. Nonclercq and P. Mathys, “Quantification of Motion Artifact Rejection Due to Active Electrodes and Driven-Right-Leg Circuit in Spike Detection Algorithms,” *IEEE Trans. Biomed. Eng.*, vol. 57, no. 11, pp. 2746–2752, Nov. 2010.
[20] J. G. Webster and J. W. Clark, Eds., *Medical instrumentation: application and design*, 4th ed. Hoboken, NJ: John Wiley & Sons, 2010.
[21] J. M. Lopez, J. C. Bohorquez, J. Bohorquez, M. A. Valderrama, and F. Segura-Quijano, “Wireless Electroencephalogram Acquisition System for Recordings in Small Animal Models,” 2013, pp. 3–4.
[22] R. T. Pivik, R. J. Broughton, R. Coppola, R. J. Davidson, N. Fox, and M. R. Nuwer, “Guidelines for the recording and quantitative analysis of electroencephalographic activity in research contexts,” *Psychophysiology*, vol. 30, no. 6, pp. 547–558, Nov. 1993.
[23] C. Borgmann, B. Roß, R. Draganova, and C. Pantev, “Human auditory middle latency responses: influence of stimulus type and intensity,” *Hear. Res.*, vol. 158, no. 1–2, pp. 57–64, Aug. 2001.
[24] L. Brown, J. van de Molengraft, R. F. Yazicioglu, T. Torfs, J. Penders, and C. Van Hoof, “A low-power, wireless, 8-channel EEG monitoring headset,” 2010, pp. 4197–4200.
[25] Y. M. Chi, Y. Wang, Y.-T. Wang, T.-P. Jung, T. Kerth, and Y. Cao, “A Practical Mobile Dry EEG System for Human Computer Interfaces,” in *Foundations of Augmented Cognition*, vol. 8027, D. D. Schmorrow and C. M. Fidopiastis, Eds. Berlin, Heidelberg: Springer Berlin Heidelberg, 2013, pp. 649–655.
[26] Chin-Teng Lin, Chun-Hsiang Chuang, Chih-Sheng Huang, Yen-Hsuan Chen, and Li-Wei Ko, “Real-time assessment of vigilance level using an innovative Mindo4 wireless EEG system,” 2013, pp. 1528–1531.
[27] Chin-Teng Lin *et al.*, “Wireless and Wearable EEG System for Evaluating Driver Vigilance,” *IEEE Trans. Biomed. Circuits Syst.*, vol. 8, no. 2, pp. 165–176, Apr. 2014.

5 Annex 1. Visual Unit Display

For experimentation, a visual unit display (VDU) was designed and implemented. This device is formed by an array of 18 horizontal bars, with a size of approximately 33 cm x 23 cm. Its electrical, mechanical and visual design followed the guidance of the VEP standard from the International Society for Clinical Electrophysiology of Vision (ISCE) in its 2009 review [1].

CRTs or computer screens are not suitable as VDUs due to their refreshing rate, which usually is in the same range of interest for the high rate stimulation VEP procedures explained before. An alternative, based the work of Toft-Nielsen et al. [2] was implemented, having two independent regions of stimulation. A small one located in the center, with a visual angle smaller than 8 ° and a outer region of approximately 15 °. Figure 5.1 shows a basic diagram of the VDU.

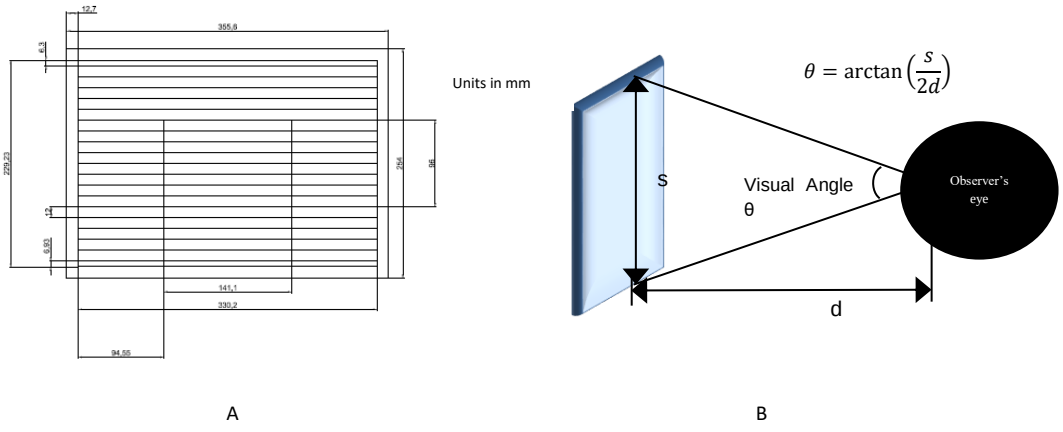

Figure 5.1 a) Blueprint of the VDU. b) Visual angle

5.1 Specifications

Some of the main properties of the VDU, following the standard and other design restrictions are listed below

- Field of vision > 15° and an aspect ratio less or equal to 4:3:15'' ≈ 33 x 23 cm
- Luminance and contrast especifications
  - Luminance: 40-60 cd m^{-2}
  - Relative contrast > 80%
- Bars with a visual angle of 1°
- Ilumination elements
  - LEDs strips from Hitlights (SMD3528-60LED/M http://www.hitlights.com/ls3528-30-group.html)
  - 12V/2A, color temperature 6000K (Cool White)
- Control system
  - Microcontroller based for synchronization with external trigger.

- Maximum stimulation rate: 100Hz
- 2 types of stimulation: flash and pattern-reversal

The Figure 5.2 shows an internal block diagram.

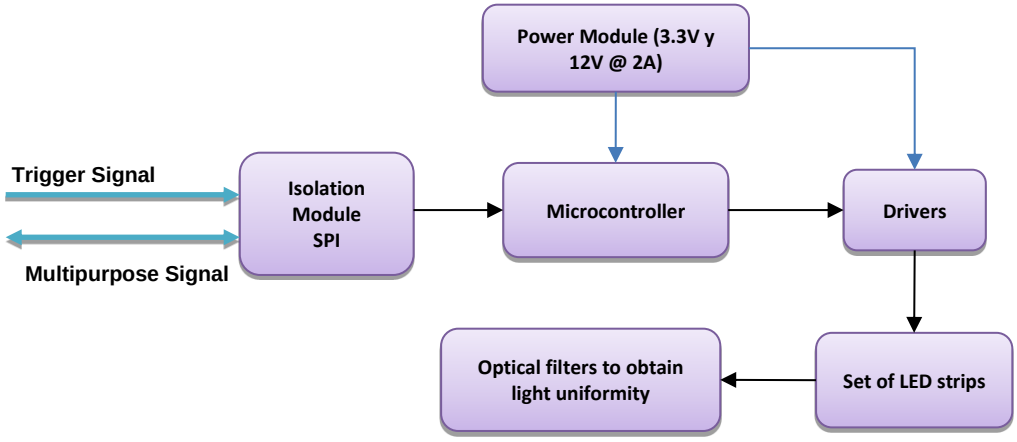

Figure 5.2. Internal Block diagram of the VDU. Is formed by fiver modules: Power Module, isolation, microcontroller, drivers and optical filters.

5.1.1 Isolation Module

VDU is connected to a wall power outlet, through an AC/DC converter. It receives a synchronization signal, usually from a computer or an EEG acquisition system, connected to the subject. For this reason, an isolation module is used, to avoid possible accidents.

5.1.2 Power Module

It delivers power to the drivers (12 V) and to the microcontroller module (3.3 V) using voltage regulators along with basic EM filters.

5.1.3 Microcontroller

Is in charge of controlling contrast and luminance through PWM channels connected to the driver module. In addition, it receives trigger signals to deliver the stimuli to the subject. Trigger signals are digital raising edges, detected by asynchronous interruption in the microcontroller.

5.1.4 Drivers

This module is formed by fast gates, capable of providing up to 2 A to a load, receiving digital signals. Drivers count with enable pins, allowing turning off completely regions or bars.

5.1.5 Optical filters

This stage avoids the perception of individual light sources, performing a low pass filtering to make a uniform illuminated surface. Is based on semi-translucid paper.

5.2 References

[1] J. V. Odom *et al.*, “ISCEV standard for clinical visual evoked potentials (2009 update),” *Doc. Ophthalmol.*, vol. 120, no. 1, pp. 111–119, Feb. 2010.

[2] J. Toft-Nielsen, J. Bohorquez, and O. Ozdamar, “Innovative pattern reversal displays for visual electrophysiological studies,” 2011, pp. 2009–2012.